



Turbulence Modelling from RANS to DNS and LES

Centre Tecnològic de Transferència de Calor (CTTC)
Universitat Politècnica de Catalunya (UPC)
(www.cttc.upc.edu)

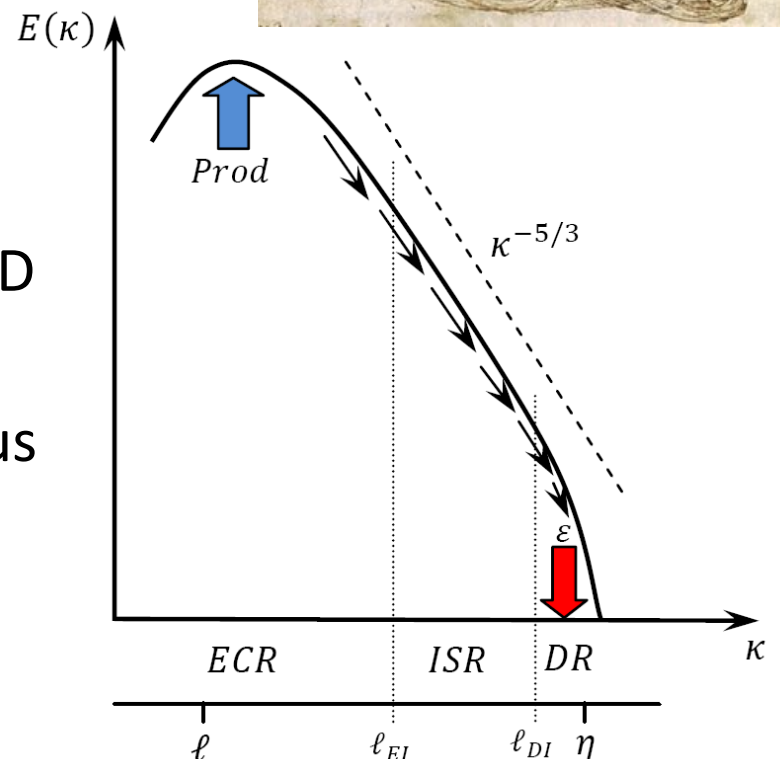
Contents

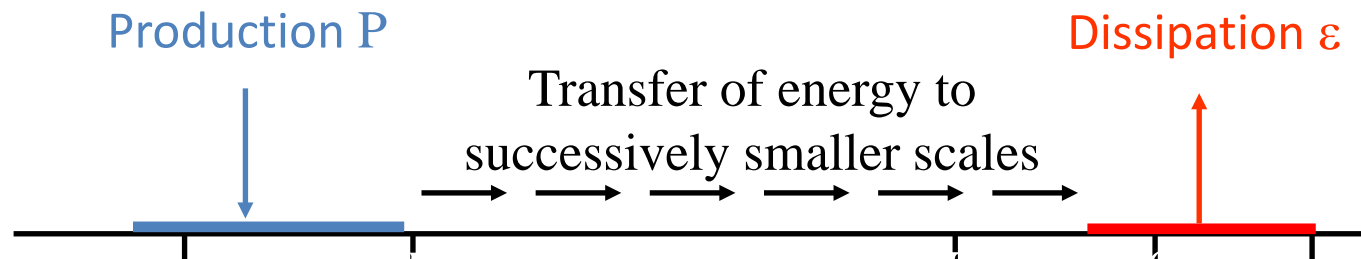
- Introduction
- Reynolds Averaged Navier Stokes (RANS) Modelling
- Direct Numerical Simulation (DNS)
- Large Eddy Simulation (LES) and Regularization Modelling (RGM)
- Conclusions

Note: Unless otherwise indicated, all the results presented in this document have been obtained by the CTTC (UPC). Most of these results can be viewed in more detail at the references indicated at <http://www.cttc.upc.edu/node/38>.

Introduction to turbulence physics

- Turbulence is the usual state of motion of fluids except at low Reynolds numbers
- At high Reynolds numbers the non-linearity of the advection process leads to instabilities making the flow unsteady and 3D
- Turbulence contains a continuous spectrum of scales.

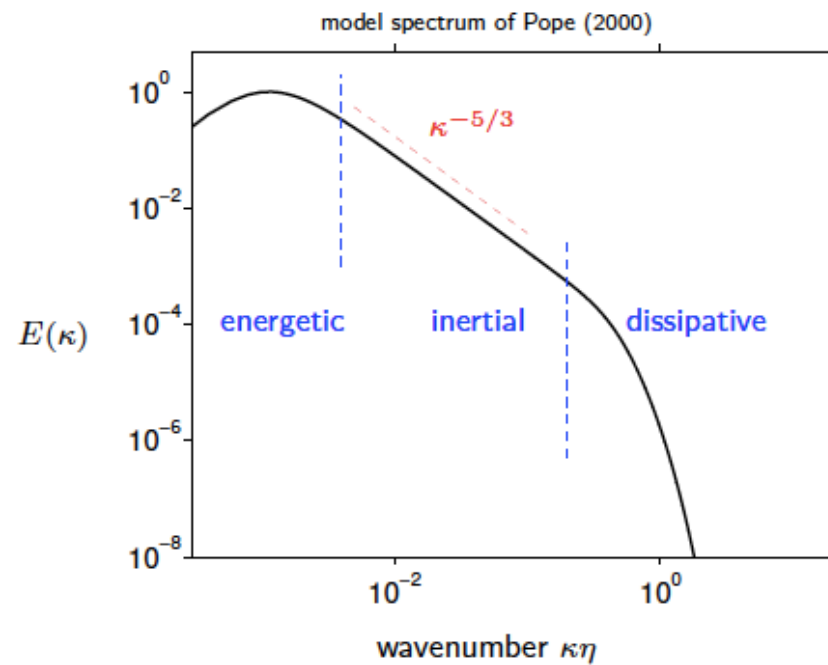




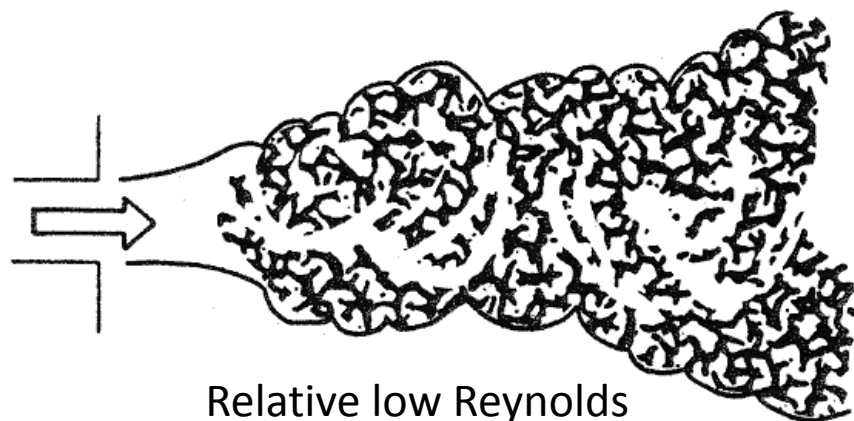
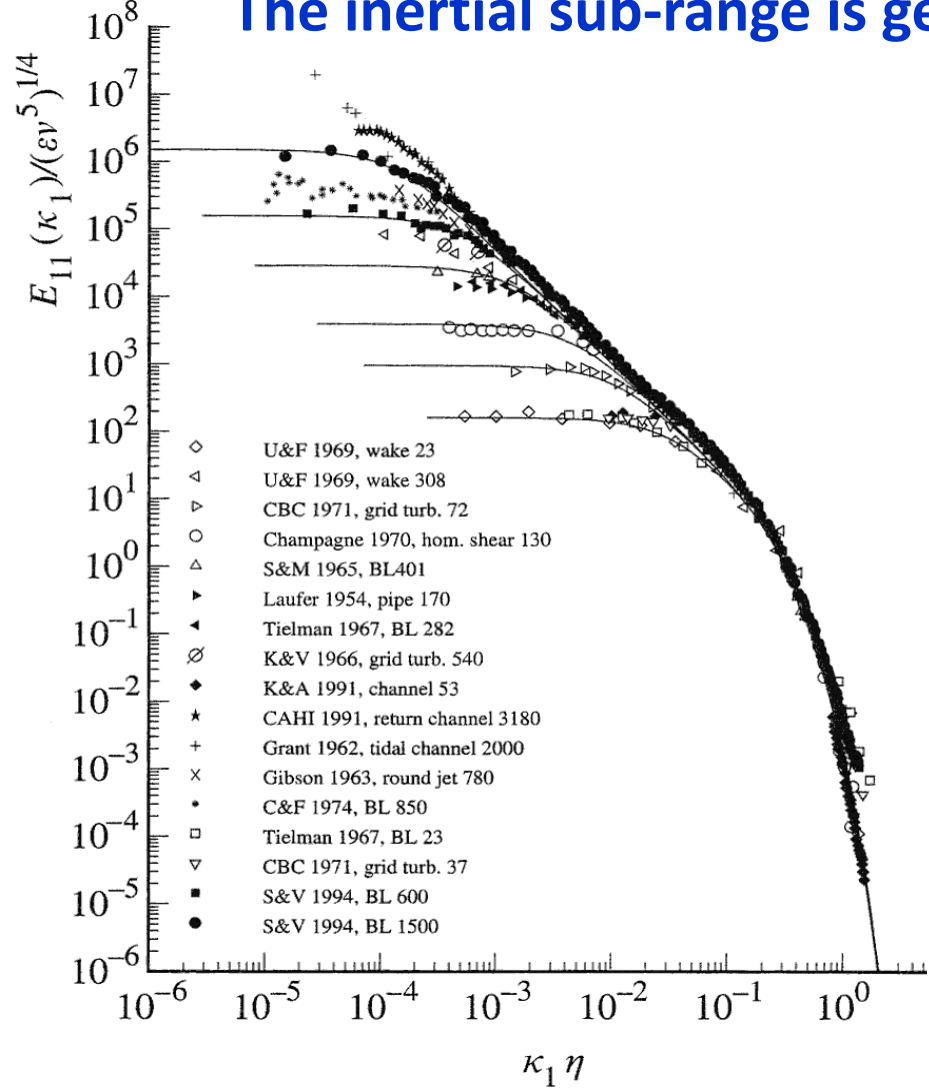
Energy containing range

Inertial subrange

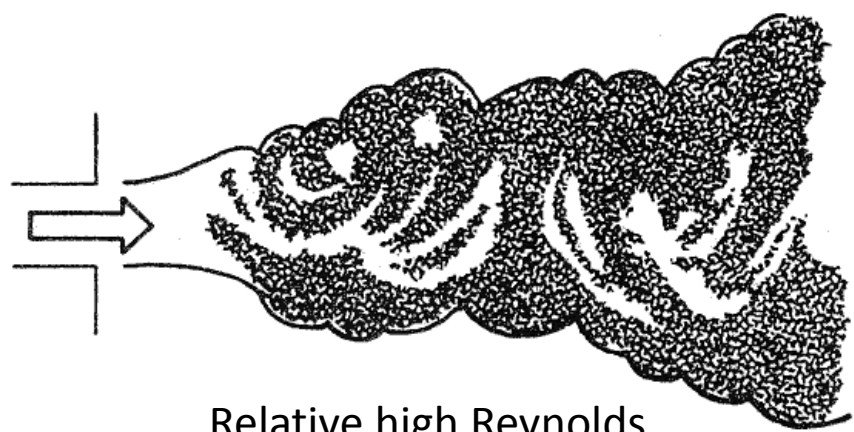
Dissipation range



The inertial sub-range is general and “case” independent

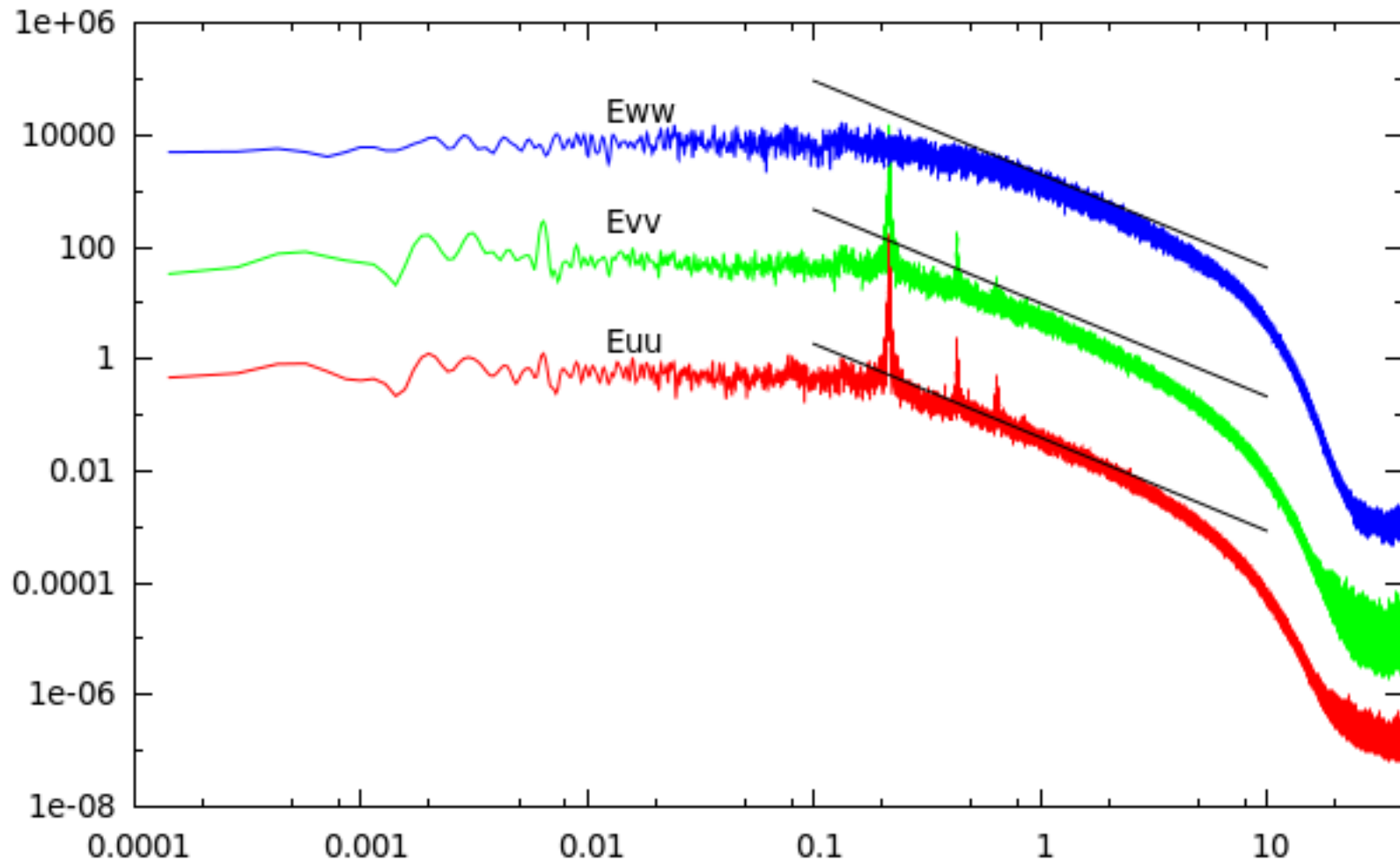


Relative low Reynolds number



Relative high Reynolds number

At the inertial sub-range the turbulence is homogeneous

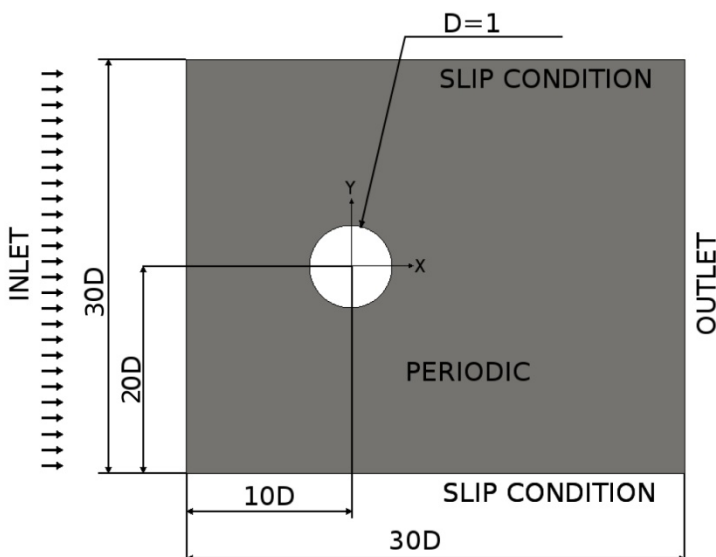


Spectral distribution of the fluctuating velocity components ($u'u'$, $v'v'$, $w'w'$) in the wake of a bluf body (cylinder)

The energy containing range is “case” dependent

Key factors in the **Production** of energy are:

- Boundary conditions
- Geometry of the problem
- Large scale dynamics



Example:

- Flow over a circular cylinder
- $Re = 5000$
- The wall of the cylinder can be rigid or rotating at different non-dimensional angular velocities, α

We change boundary conditions only



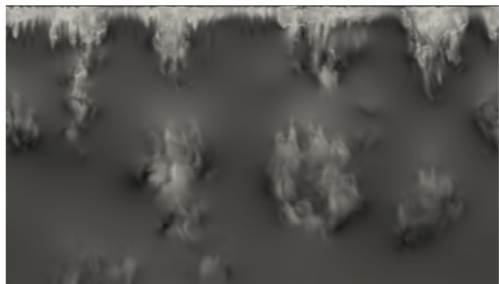
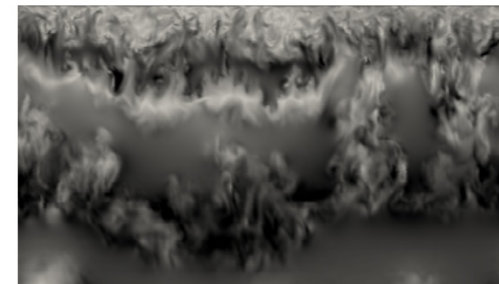
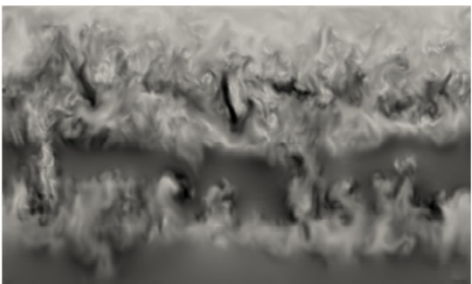
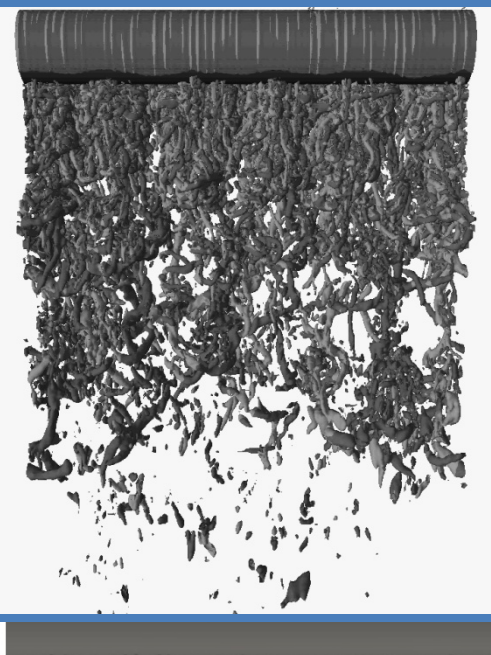
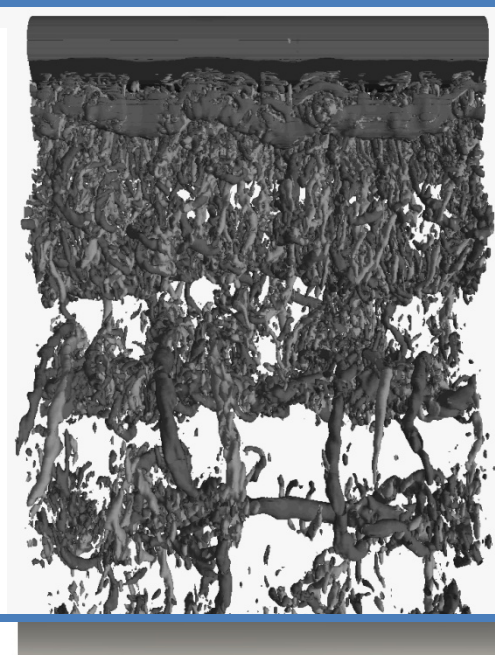
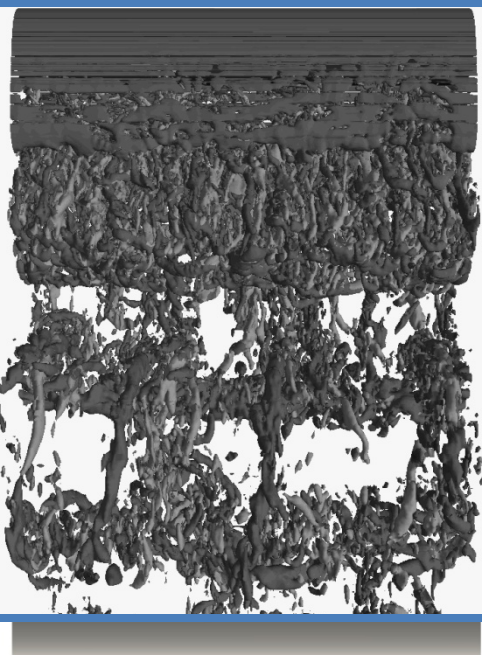
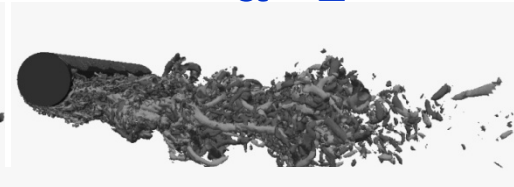
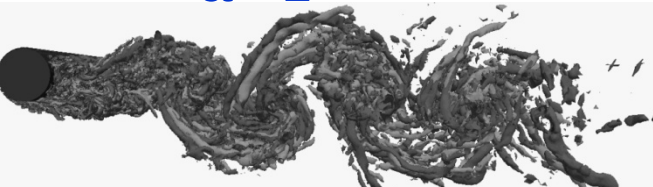
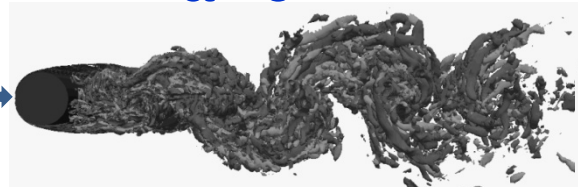
Hence we alter the Production

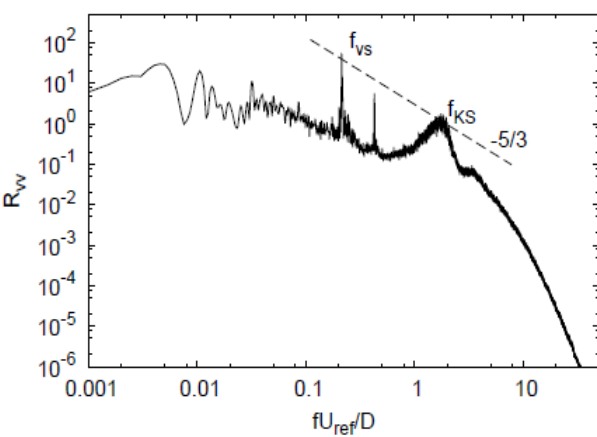
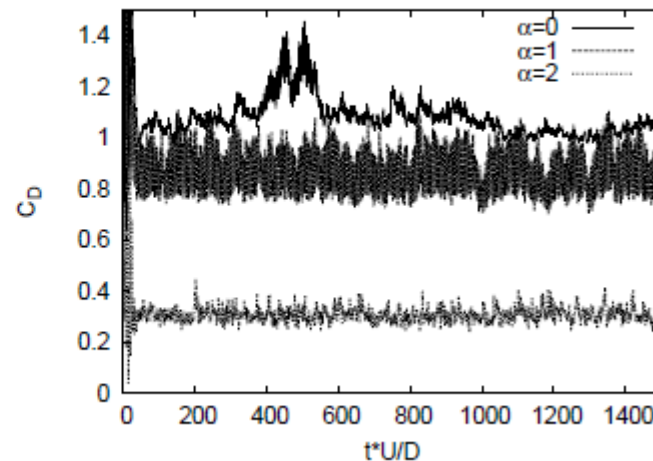
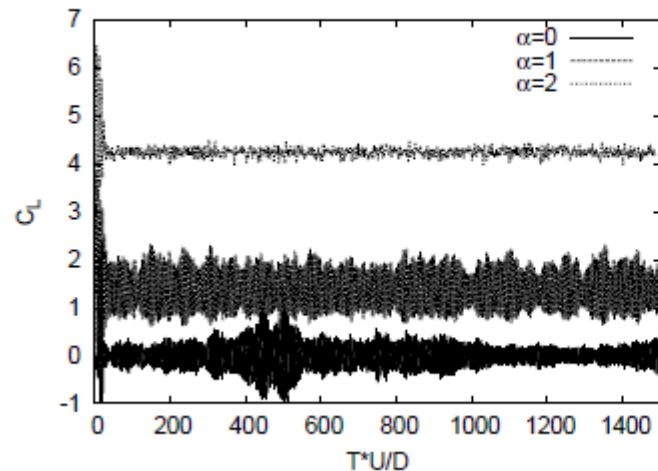
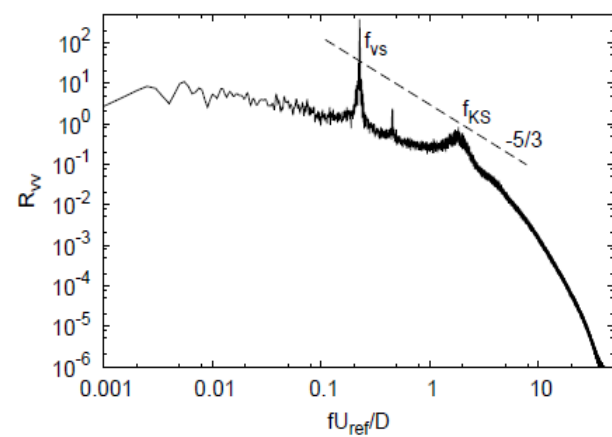
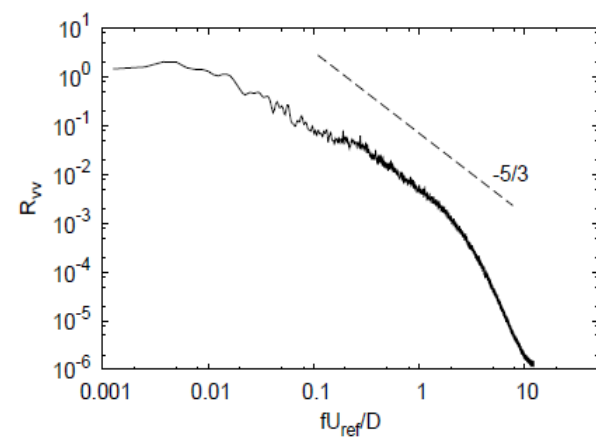
CTTC (UPC)

$\alpha = 0$

$\alpha = 1$

$\alpha = 2$



(a) $\alpha = 0$ (b) $\alpha = 1$ (c) $\alpha = 2$

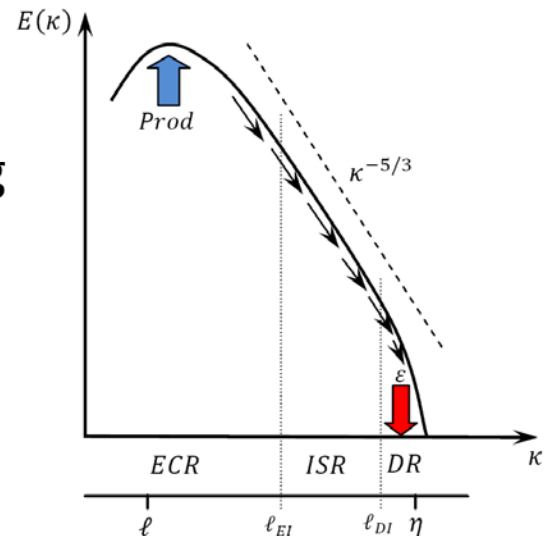
Introduction to modelling

- Laminar and turbulent flows are governed by the same equations (continuum hypothesis is also suitable for turbulence)
- NS equations for incompressible Newtonian fluids

$$\nabla \cdot \mathbf{u} = 0$$

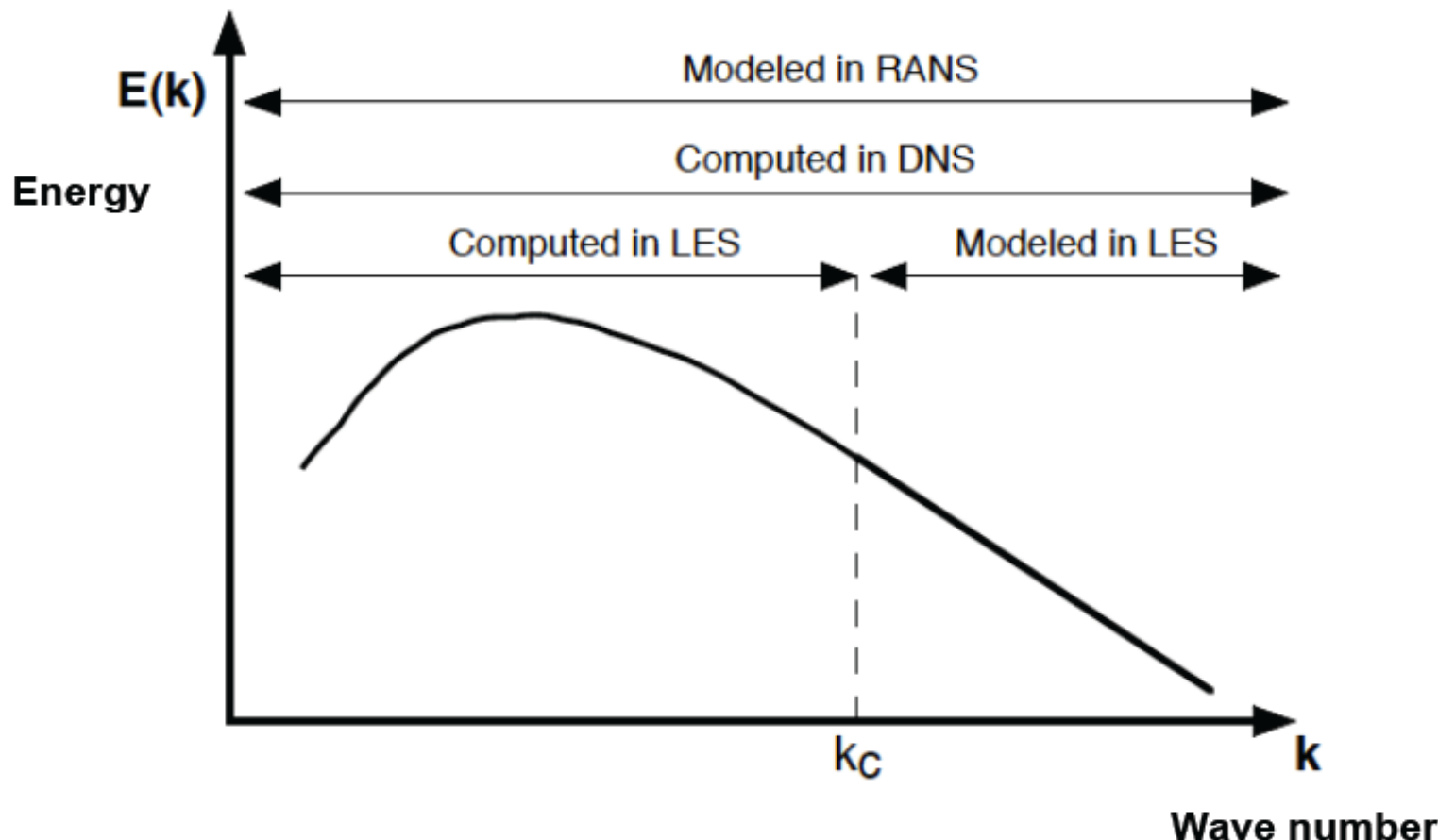
$$\frac{\partial \mathbf{u}}{\partial t} + (\mathbf{u} \cdot \nabla) \mathbf{u} = -\frac{1}{\rho} \nabla p + \nabla \cdot (2\nu \mathbf{S}) - \beta(T - T_o) \mathbf{g}$$

$$\frac{\partial T}{\partial t} + \mathbf{u} \cdot \nabla T = \frac{\lambda}{\rho c_p} \nabla^2 T$$

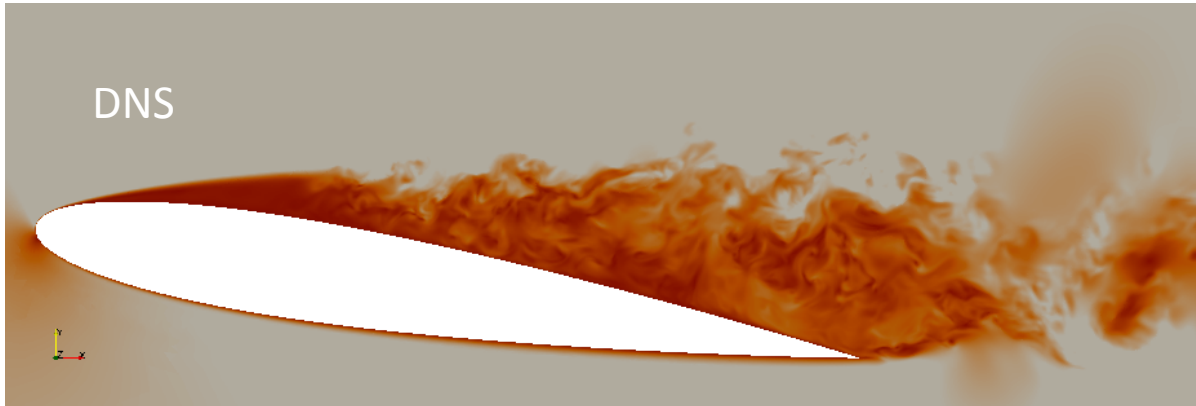


- DNS vs. LES vs. RANS

DNS vs LES vs RANS



DNS

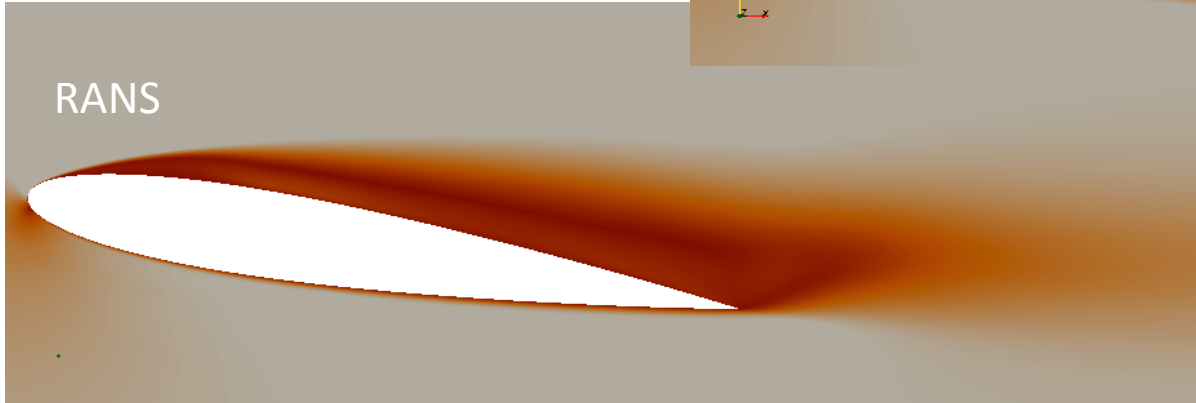


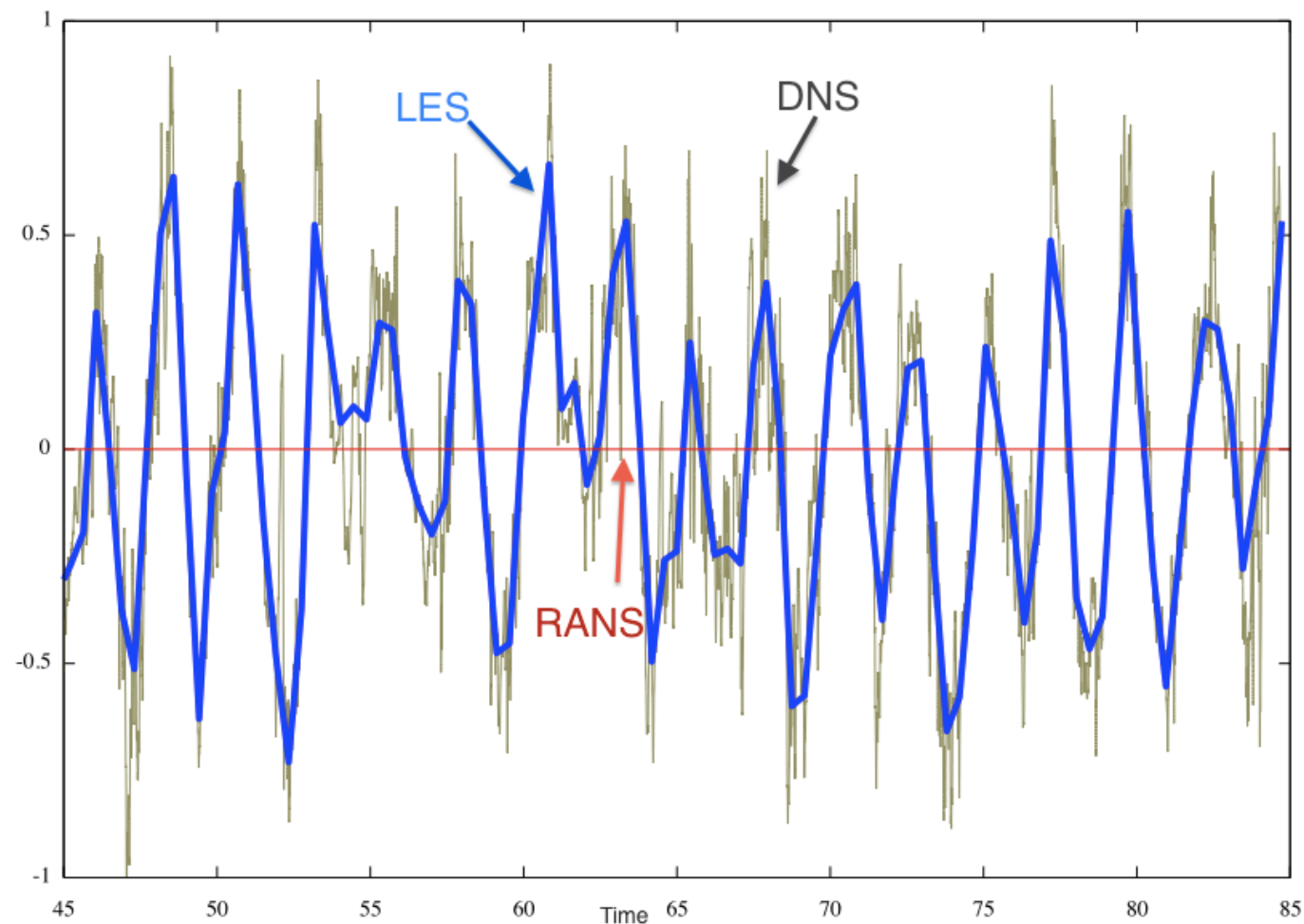
Flow past a NACA0012
airfoil at $\text{AoA}=9^\circ \text{ Re}=5\text{e}4$

LES



RANS





Time evolution of the velocity at a given location (NACA0012)

RANS – Mathematical formulation – Reynolds Averaged Navier-Stokes Equations (RANS)

- Instantaneous variables are expressed as:

$$\phi(x, t) = \bar{\phi}(x, t) + \phi'(x, t) = \frac{1}{\Delta t} \int_t^{t+\Delta t} \phi(x, t) dt + \phi'(x, t)$$

- RANS equations:

$$\nabla \cdot \bar{\mathbf{u}} = 0$$

$$\frac{\partial \bar{\mathbf{u}}}{\partial t} + (\bar{\mathbf{u}} \cdot \nabla) \bar{\mathbf{u}} = -\frac{1}{\rho} \nabla \bar{p} + \nabla \cdot (2\nu \bar{\mathbf{S}} - \overline{\mathbf{u}'\mathbf{u}'}) - \beta(\bar{T} - T_o) \mathbf{g}$$

$$\frac{\partial \bar{T}}{\partial t} + \bar{\mathbf{u}} \cdot \nabla \bar{T} = \nabla \cdot \left(\frac{\lambda}{\rho c_p} \nabla \bar{T} - \overline{\mathbf{u}'T'} \right)$$

RANS – Mathematical formulation – Hierarchy of turbulence models

- Differential Reynolds Stress Models (DRSM): $\frac{D(\overline{u'u'})}{Dt} \approx \dots; \quad \frac{D(\overline{u'T})}{Dt} \approx \dots$
- Algebraic Reynolds Stress Models (ARSM): $f(\overline{u'u'}, \dots) \approx 0; \quad f(\overline{u'T}, \dots) \approx 0$
- **Explicit Algebraic Reynolds Stress Models (EARSM):** $\overline{u'u'} = \dots; \quad \overline{u'T'} = \dots$
- **Eddy Viscosity Models (LEVM and NLEVM):**

$$\overline{u'u'} - \frac{2}{3}k\mathbf{I} \approx -v_t(\nabla \overline{\mathbf{u}} + \nabla \overline{\mathbf{u}}^*); \quad \overline{u'T'} \approx -\frac{v_t}{\sigma_T} \nabla \bar{T}$$

$$\begin{aligned} \frac{\overline{u'u'}}{k} - \frac{2}{3}\mathbf{I} &\approx -2C_\mu f_\mu S + \beta_1 \left(\mathbf{S} \cdot \mathbf{S} - \frac{1}{3}[\mathbf{S} \cdot \mathbf{S}] \mathbf{I} \right) + \beta_2 (\mathbf{W} \cdot \mathbf{S} - \mathbf{S} \cdot \mathbf{W}) + \beta_3 \left(\mathbf{W} \cdot \mathbf{W} - \frac{1}{3}[\mathbf{W} \cdot \mathbf{W}] \mathbf{I} \right) - \gamma_1 [\mathbf{S} \cdot \mathbf{S}] \mathbf{S} \\ &\quad - \gamma_2 [\mathbf{W} \cdot \mathbf{W}] \mathbf{S} - \gamma_3 \left(\mathbf{W} \cdot \mathbf{W} \cdot \mathbf{S} + \mathbf{S} \cdot \mathbf{W} \cdot \mathbf{W} - [\mathbf{W} \cdot \mathbf{W}] \mathbf{S} - \frac{2}{3} [\mathbf{W} \cdot \mathbf{S} \cdot \mathbf{W}] \mathbf{I} \right) - \gamma_4 (\mathbf{W} \cdot \mathbf{S} \cdot \mathbf{S} - \mathbf{S} \cdot \mathbf{S} \cdot \mathbf{W}) \end{aligned}$$

where: $v_t = C_\mu f_\mu \frac{k^2}{\varepsilon} = C_\mu^* f_\mu^* \frac{k}{\omega}; \quad \sigma_T = 0.9$

RANS – Mathematical formulation – Turbulent transport equations

- Two extra transport equations are needed to obtain k and its dissipation rate (ε or ω)

$$\frac{\partial k}{\partial t} + \bar{\mathbf{u}} \cdot \nabla k = \nabla \cdot \left[\left(v + \frac{v_t}{\sigma_k} \right) \nabla k \right] + P_k + G_k - \varepsilon$$

$$\frac{\partial \tilde{\varepsilon}}{\partial t} + \bar{\mathbf{u}} \cdot \nabla \tilde{\varepsilon} = \nabla \cdot \left[\left(v + \frac{v_t}{\sigma_\varepsilon} \right) \nabla \tilde{\varepsilon} \right] + f_1 C_{\varepsilon 1} \frac{\tilde{\varepsilon}}{k} P_k + f_3 C_{\varepsilon 3} \frac{\tilde{\varepsilon}}{k} G_k - f_2 C_{\varepsilon 2} \frac{\tilde{\varepsilon}^2}{k} + E + Y_c$$

$$\frac{\partial \omega}{\partial t} + \bar{\mathbf{u}} \cdot \nabla \omega = \nabla \cdot \left[\left(v + \frac{v_t}{\sigma_\omega} \right) \nabla \omega \right] + f_{\omega 1} C_{\omega 1} \frac{\omega}{k} P_k + f_{\omega 2} C_{\omega 2} \frac{\omega}{k} G_k - \beta \omega^2$$

where,

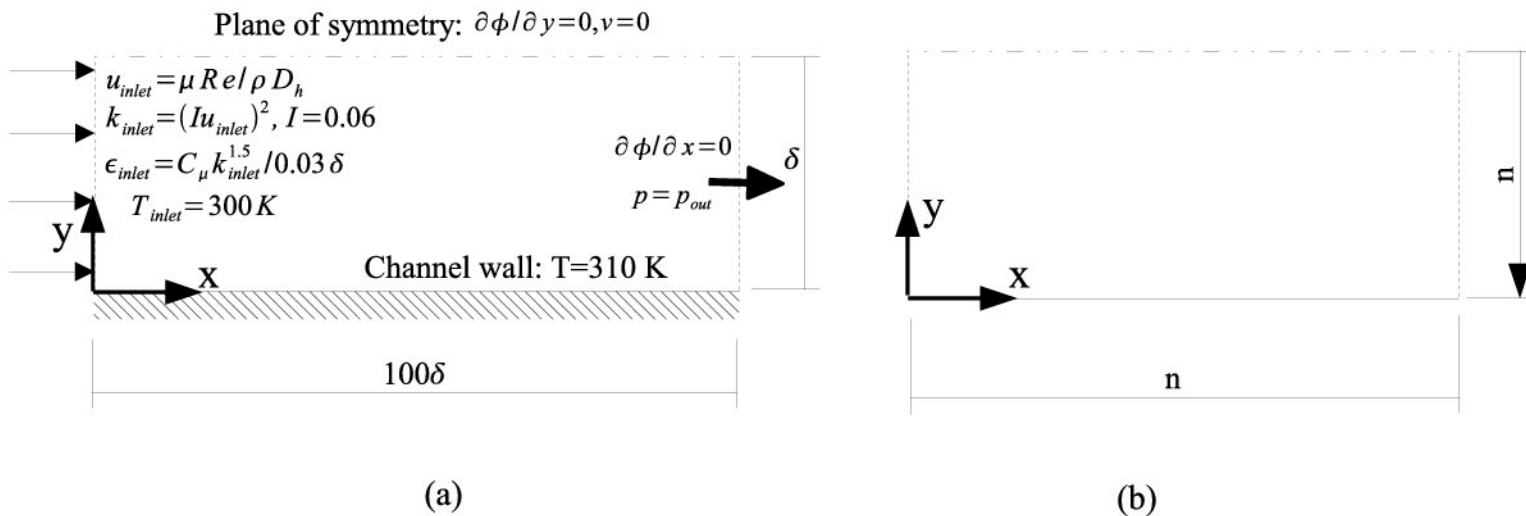
$$\tilde{\varepsilon} = \varepsilon + D; \quad P_k = -\overline{\mathbf{u}' \mathbf{u}'} : \nabla \bar{\mathbf{u}}; \quad G_k = -\beta \mathbf{g} \cdot \left(-\frac{\mu_t}{\sigma_T} \nabla \bar{T} \right) \text{ (SGDH)}; \quad G_k = -\beta \mathbf{g} \cdot \left(-\frac{3}{2} \frac{C_\mu f_\mu}{\sigma_T} \overline{\mathbf{u}' \mathbf{u}'} \cdot \nabla \bar{T} \right) \text{ (GGDH)}$$

RANS – Mathematical formulation – Turbulent models tested

	$k-\varepsilon$	$k-\omega$
LEVM	IL Ince-Launder, 1989 GPC Goldberg-Peroomian-Chakravarthy, 1998	WX Wilcox, 1993 WXT Wilcox, 1994 WXCD Wilcox, 1998 PDH+D Peng, Davidson and Holmberg, 1999
NLEVM	CLS Craft-Launder-Suga, 1996	LAR Larsson, 1997 AJL Abe-Jang-Leschziner, 2003
EARSM	AMGS Abid-Morrison-Gatski-Speziale, 1996	ARG Abid-Rumsey-Gatski, 1995 WJO Wallin-Johanson, 2000

RANS – Examples – Plane channel flow

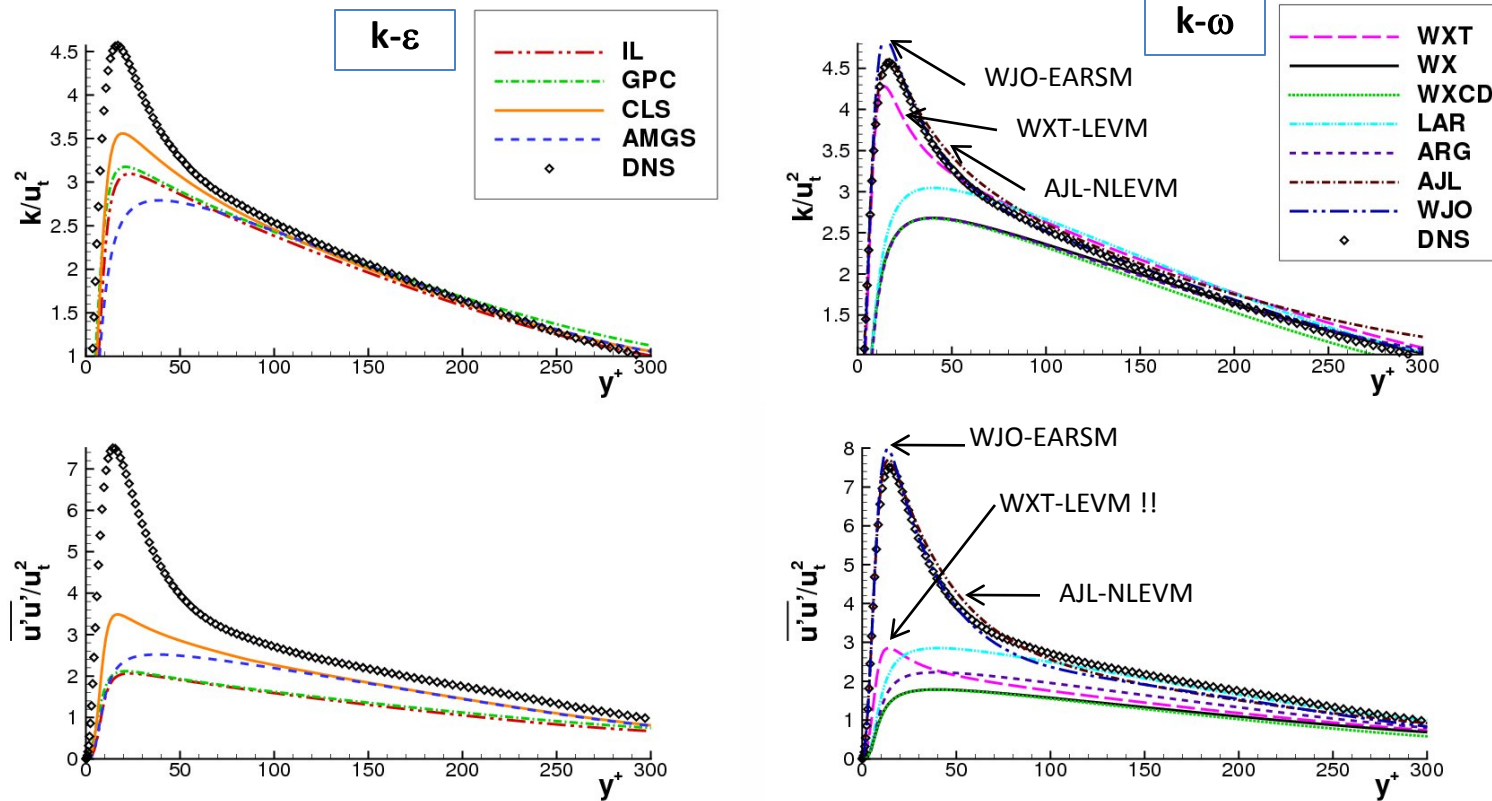
- Geometry, boundary conditions and computational domain



- Three cases: i) $Re_t=180$ ($Re_{Dh} \approx 5640$); ii) $Re_t=395$ ($Re_{Dh} \approx 13800$); iii) $Re_t=590$ ($Re_{Dh} \approx 21700$).
 - DNS data by R.Moser et al. (Physics of Fluids 11:943-945, 1999).

RANS – Examples – Plane channel flow ($Re_\tau = 395$, $Re_{2\delta} \approx 13800$)

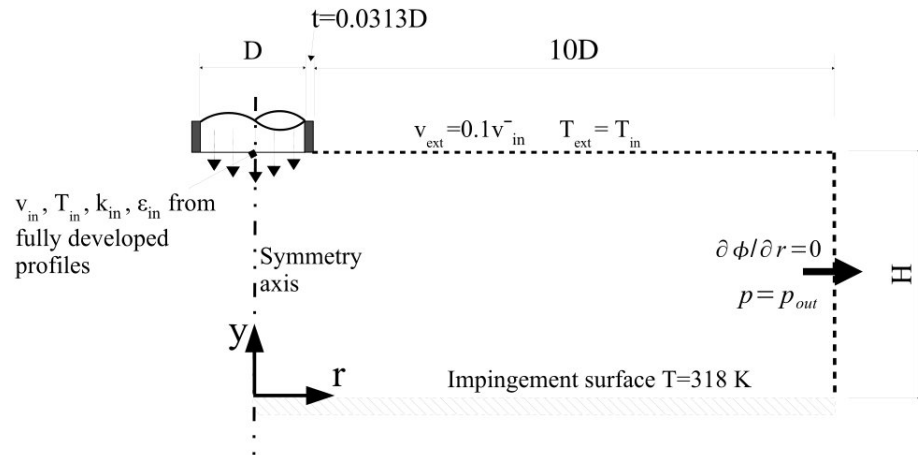
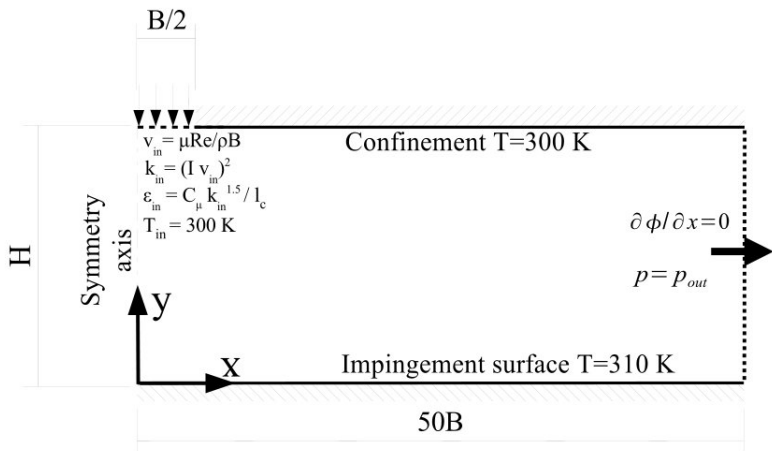
- Turbulent kinetic energy and streamwise Reynolds stresses



- k : good performance of AJL ($k\omega$ -NLEVM), WJO ($k\omega$ -EARSM), WXT ($k\omega$ -LEVM)
- $\text{avg}(u'u')$: well predicted by AJL ($k\omega$ -NLEVM), WJO ($k\omega$ -EARSM)
- In general, high-order $k\omega$ models show better behaviour than $k\epsilon$ models

RANS – Examples – Plane and round impinging jet

- Geometry, boundary conditions and computational domain



Plane impinging jet. Three cases: i) $Re_B=10200$, $H/B=2.6$; ii) $Re_B=20000$, $H/B=4.0$; iii) $Re_B=30000$, $H/B=9.2$. $Pr=0.71$.

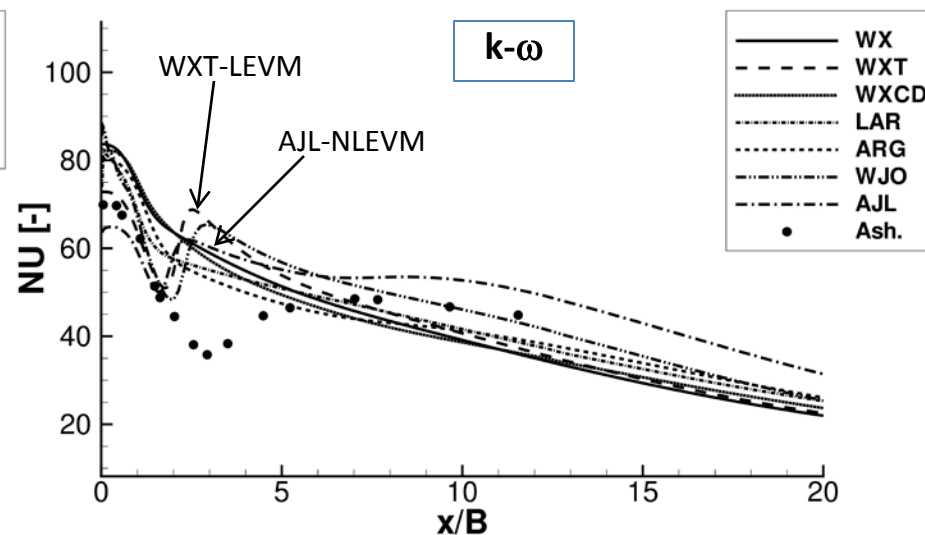
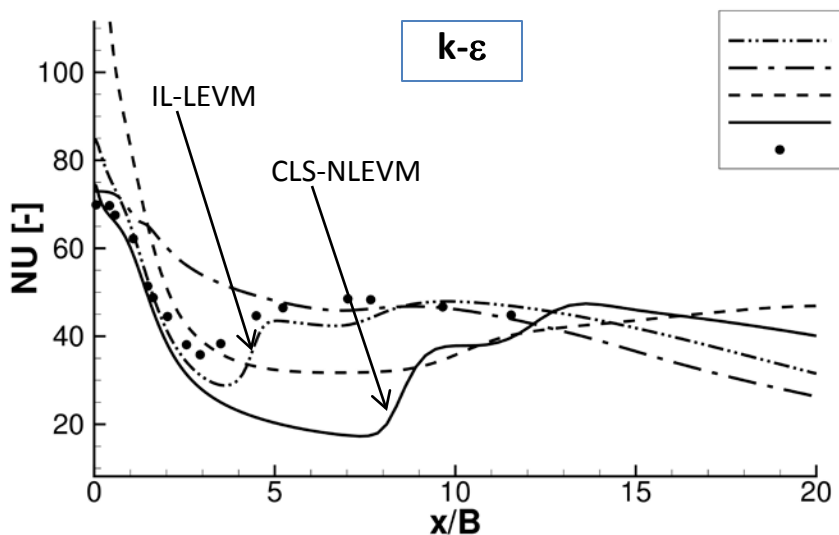
Experimental data by Heiningen (PhD Thesis, 1982) (i); Ashforth-Frost (Exp. Therm. Fluid Sc., 14:60-67, 1997) (ii); Zhe and Modi (J. Fluid Eng., 123:112-120, 2001) (ii)&(iii).

Round impinging jet. Two cases: i) $Re_D=23000$, $H/D=2$; ii) $Re_D=70000$, $H/D=6$. $Pr=0.71$.

Experimental data by Baughn and Shimizu (J. Heat Transfer, 1989) (i)&(ii) - heat transfer; Cooper et al. (Int. J. Heat Mass Transfer, 1993) (i)&(ii) - velocities.

RANS – Examples – Plane impinging jet ($Re_B=20000$, $H/B=4.0$)

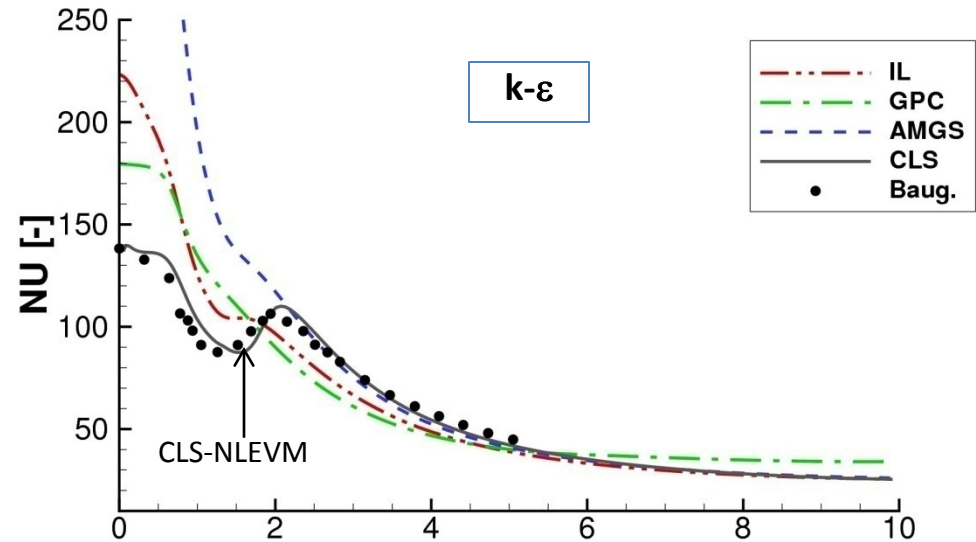
- Nusselt number at the impinging plate



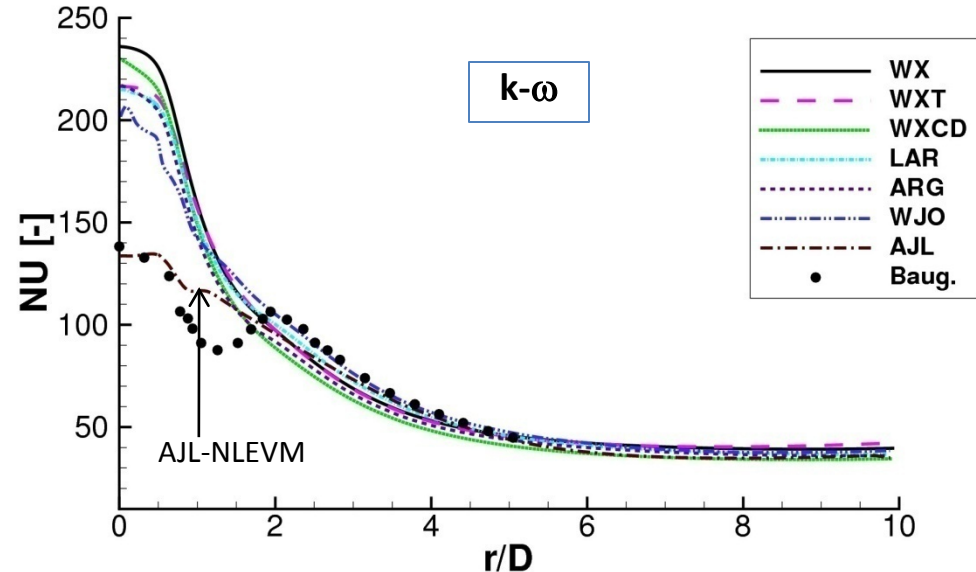
- Stagnation point: NLEVM and EARSM improve LEVM (see CLS vs. IL or LAR and ARG vs. WX). However, AMGS shows poor behaviour.
- Secondary maximum location: IL reasonably correct; CLS with delay; WXT, WJO and AJL too early

RANS – Examples – Round impinging jet ($Re_B=23000$, $H/D=2.0$)

- Nusselt number at the impinging plate

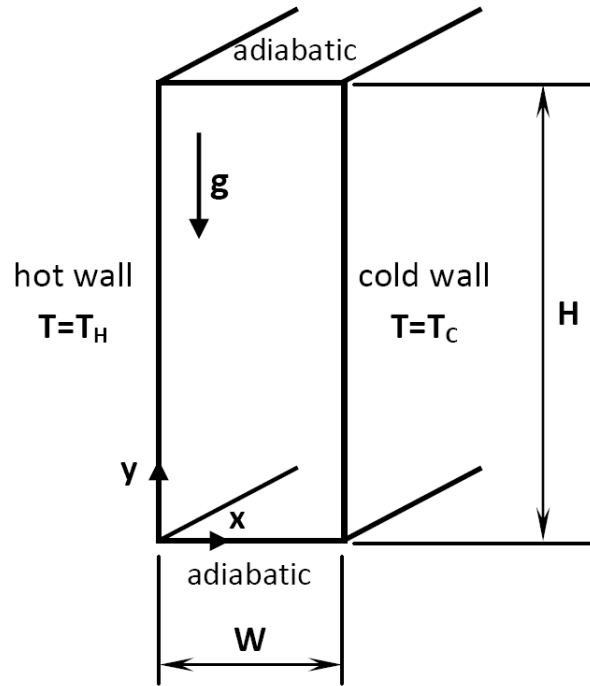


- CLS gives very good predictions.
- AJL improves LEVM predictions
- Different performance in plane and round impinging jet situations.



RANS – Examples – Differentially heated cavity

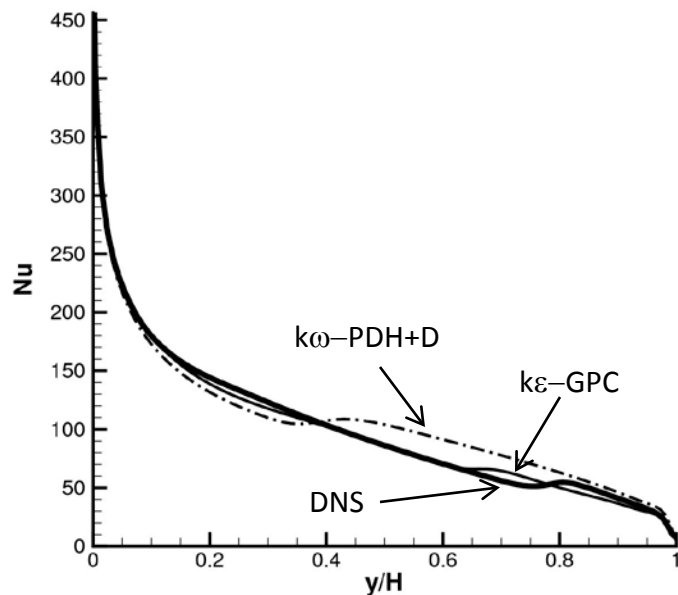
- Geometry and boundary conditions



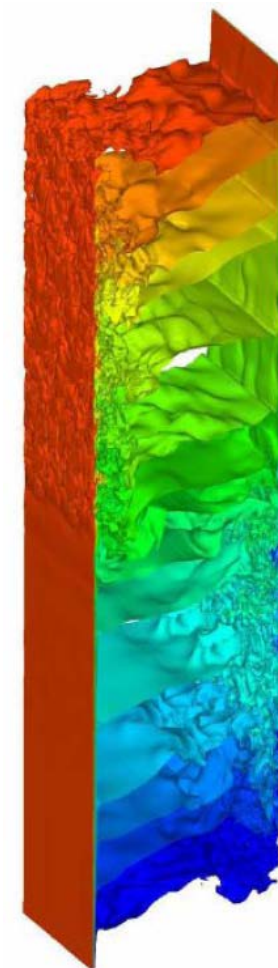
- Four cases tested: i) $A=H/W=30$ (tall cavity), $Ra_H=2.43\times10^{10}$, $Pr=0.71$; ii) $A= 5$, $Ra_H=5\times10^{10}$, $Pr=0.71$; iii) $A=4$, $Ra_H=1\times10^{10}$ and $Ra_H=1\times10^{11}$, $Pr=0.71$.
- Experiments by Daffa'alla and Betts for $A=30$ (Exp. Heat Transfer, 1996); Cheesewright et al for $A=5$ (Procc., 1986); and DNS results $A=4$ (CTTC results).

RANS – Examples – DHC ($A=4$, $Ra_H=10^{10}$)

- Nusselt number distribution at the hot wall

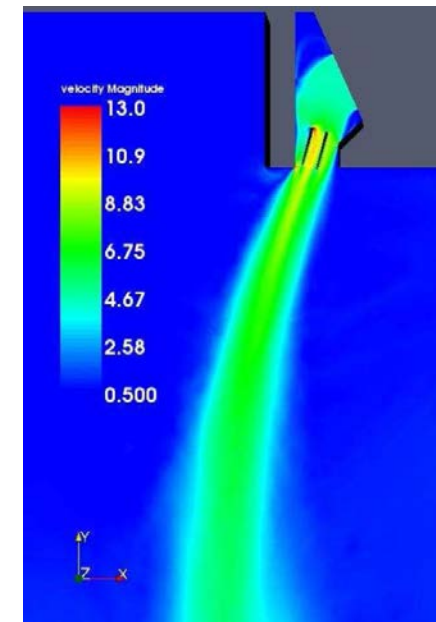
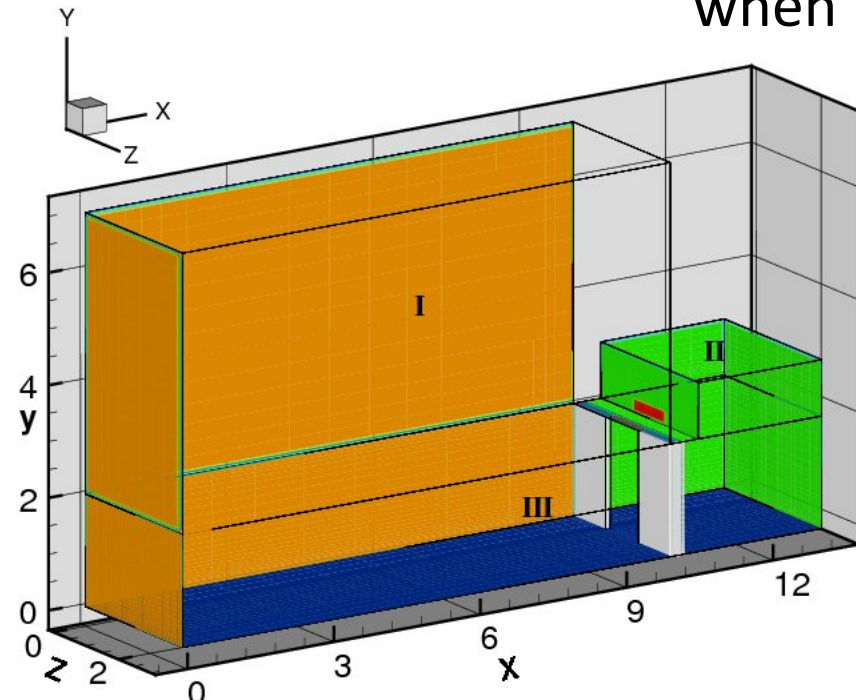


- $A=30$, all tested models (IL, GPC, WX, WXT, PDH+D) give reasonable accurate results (specially IL)
- $A=5$ and $A=4$, IL delays transition when the grid is refined (eventually the flow becomes fully laminar). WX and WXT do not present this problem but they give poor results.
- $A=5$ and $A=4$, IL delays transition when the grid is refined (eventually the flow becomes fully laminar). WX and WXT do not present this problem but they give poor results.



RANS – Examples – Industrial application. Refrigerated Space

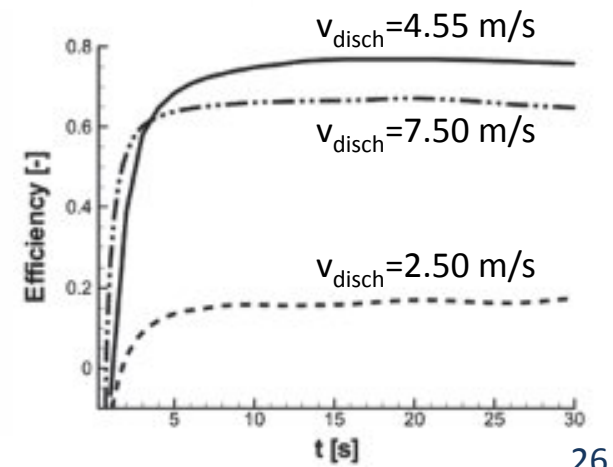
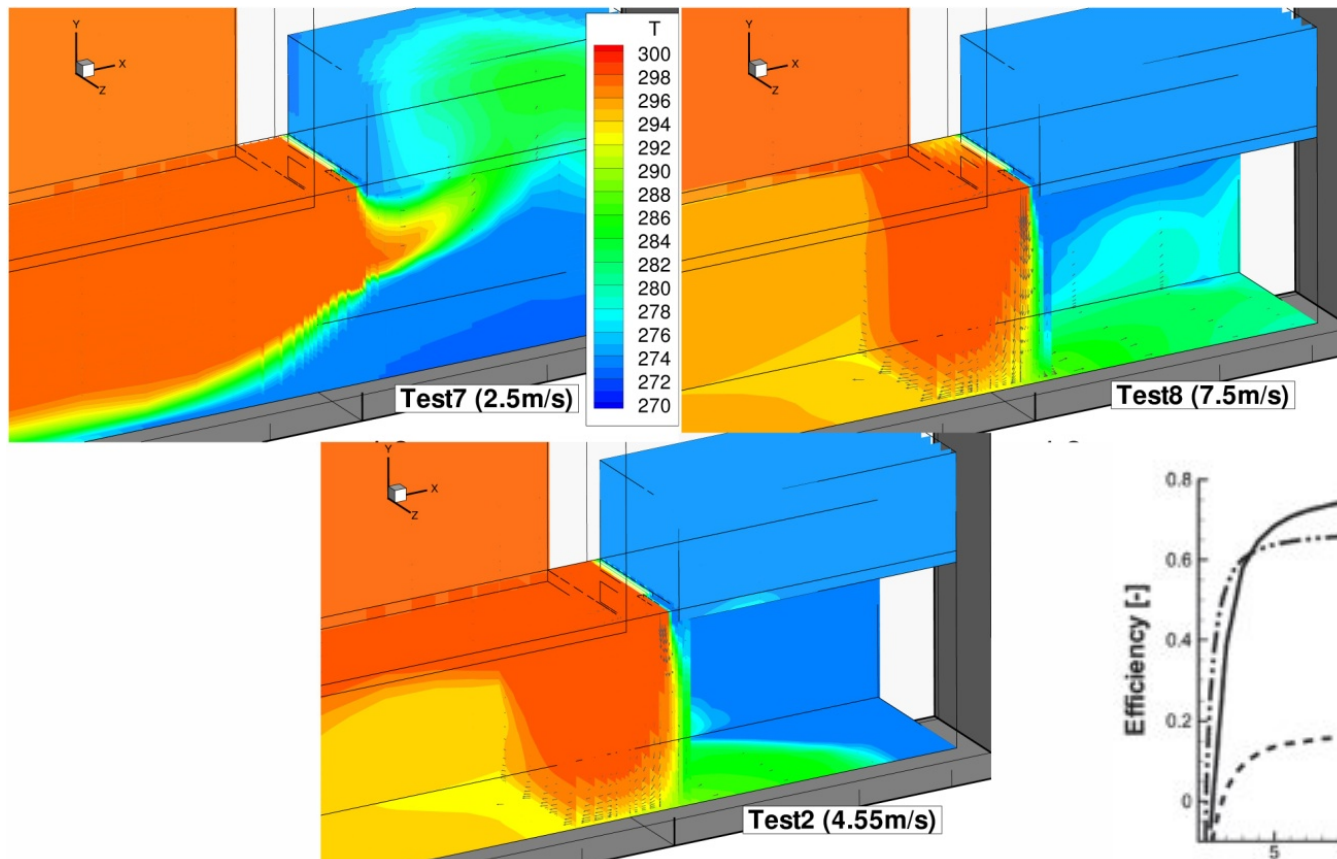
- Thermal and fluid dynamic behaviour of a refrigerated space (II) when its door is suddenly opened.



- Structured meshes using multiblock techniques
- Two grids: 21000 CVs and 107000 CVs
- Three time-steps: 0.01, 0.05 or 0.1 s
- LEVM-IL gives similar results than WXT, but better convergence

RANS – Examples – Industrial application. Refrigerated Space

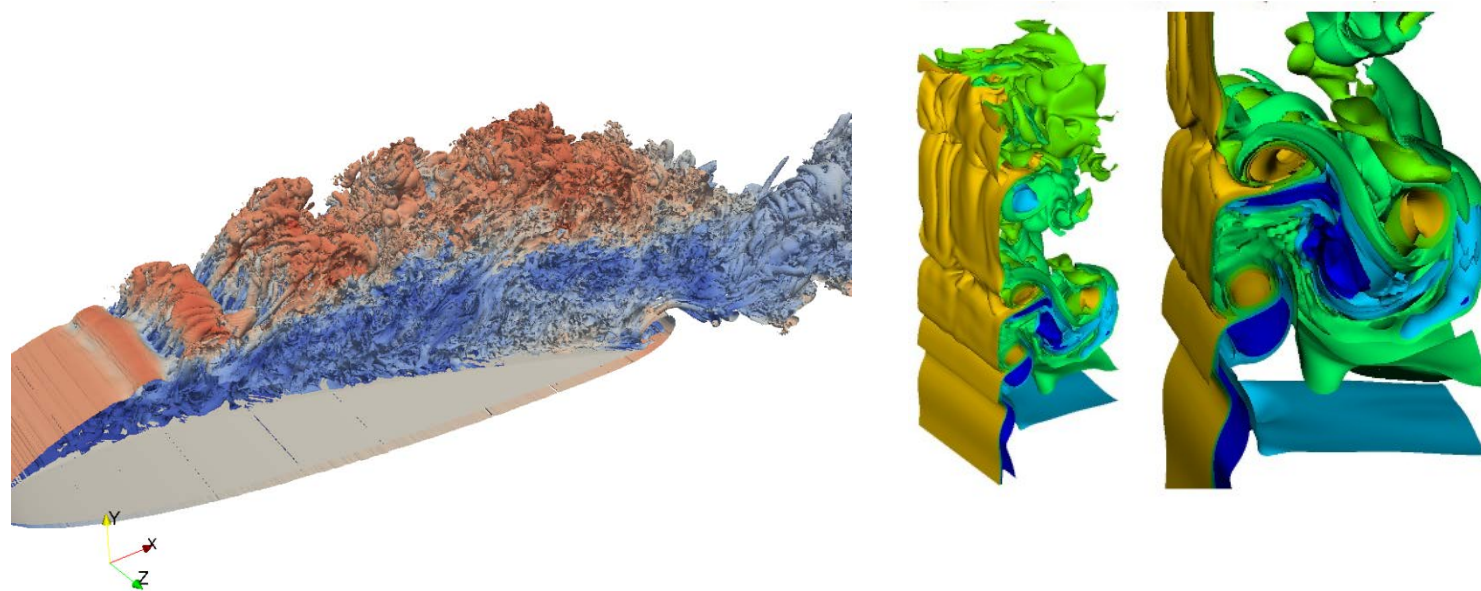
- Influence of air curtain discharge velocity considering $\alpha_{\text{disch}}=0$ and $T_{\text{disch}}=T_{\text{warm}}$ (warm air suction/discharge).



RANS modelling - Summary

- Studies of RANS modelling using well-known LEVM, NLEVM and EARSM and considering $k-\varepsilon$ as well as $k-\omega$ platforms have been performed.
- Turbulence models have been tested in different cases (channel flow, round impinging jet, plane impinging jet, differential heated cavity, industrial application)
- When using adequate meshes, $k-\omega$ models show generally higher accuracy near solid walls and better convergence and stability properties than $k-\varepsilon$ models.
- In general, EARSM and NLEVM show higher accuracy than LEVM. However, the advantage is not clear.
- RANS computations do not need very high computational resources. Currently, they are the most widely used design tool in engineering.
- There is not an “optimal” RANS model effective for all the different flows configurations analyzed

Direct Numerical Simulation (DNS) and Large Eddy Simulation (LES) Regularization Modelling (RGM)



DNS- Direct Numerical Simulation

- Finite volume discretization of the continuity, Navier-Stokes and energy equations for all of the N -CVs the domain is discretized using arbitrary collocated meshes

$$\textcolor{red}{M}_c \mathbf{u}_c = 0$$

$$\boldsymbol{\Omega}_c \frac{\partial \mathbf{u}_c}{\partial t} + \textcolor{red}{C}_c(\mathbf{u}_c) \mathbf{u}_c = \nu \textcolor{red}{D}_c \mathbf{u}_c - \rho^{-1} \boldsymbol{\Omega}_c \textcolor{red}{G}_c \mathbf{p}_c + \boldsymbol{\Omega}_c \mathbf{f}_c$$

$$\boldsymbol{\Omega}_c \frac{\partial \mathbf{T}_c}{\partial t} + \textcolor{red}{C}_c(\mathbf{u}_c) \mathbf{T}_c = \lambda \rho^{-1} c_p^{-1} \textcolor{red}{D}_c \mathbf{T}_c$$

where,

$$\mathbf{u}_c^* = \{v_{x1}, v_{x2}, \dots, v_{xN}, v_{y1}, v_{y2}, \dots, v_{yN}, v_{z1}, v_{z2}, \dots, v_{zN}\}; \quad \mathbf{p}_c^* = \{p_1, p_2, \dots, p_N\}; \quad \mathbf{T}_c^* = \{T_1, T_2, \dots, T_N\}$$

- Direct Numerical Simulation (DNS) solves all relevant scales in turbulent flow. There are no model approximations.
- DNS approach: $5xN$ equations with $5xN$ unknowns (\mathbf{u}_c , \mathbf{p}_c , \mathbf{T}_c) must be solved at each Δt
- DNS demands accurate numerical schemes (guided by theory) and parallelization techniques.

DNS - High Performance Computing is a must!



Curie - TCGG



MareNostrum - BSC



Magerit - CeSViMa

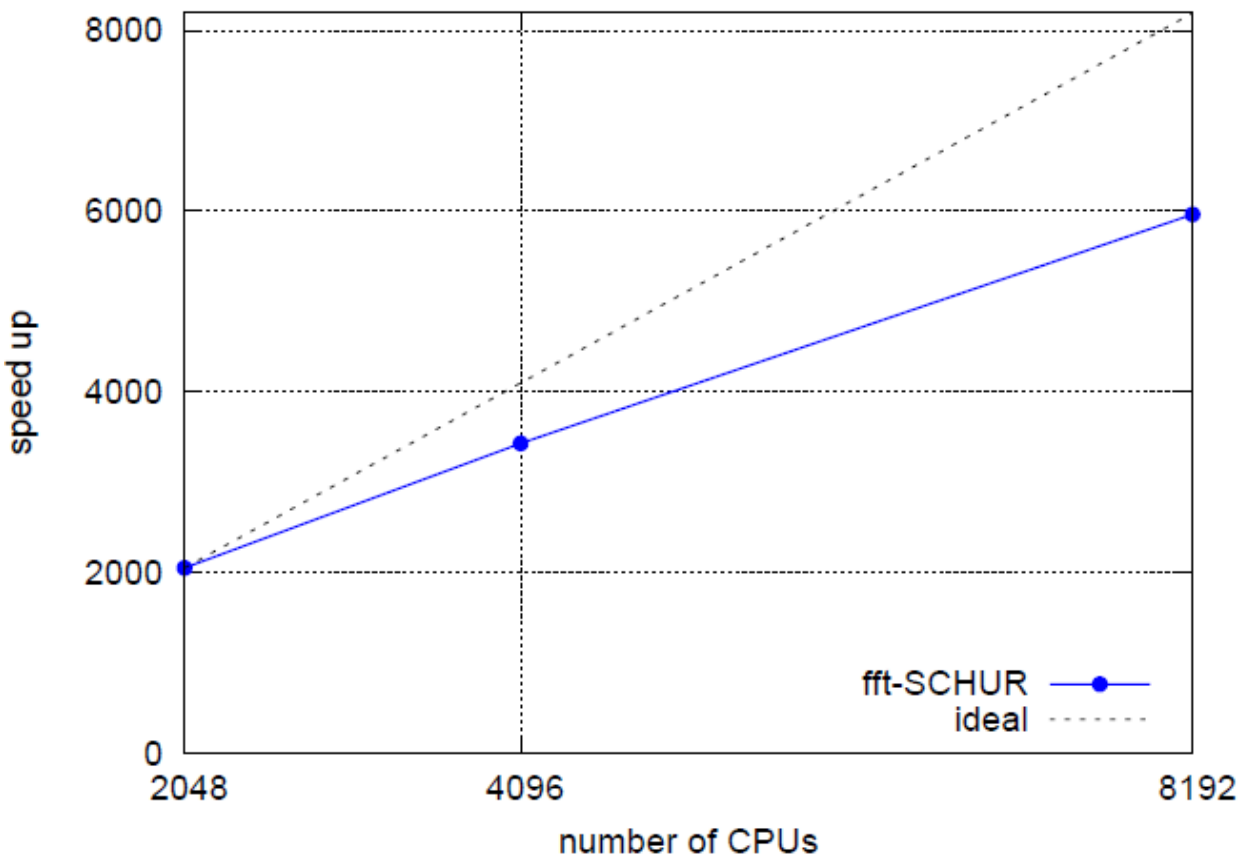


Lomonosov - RCC MSU



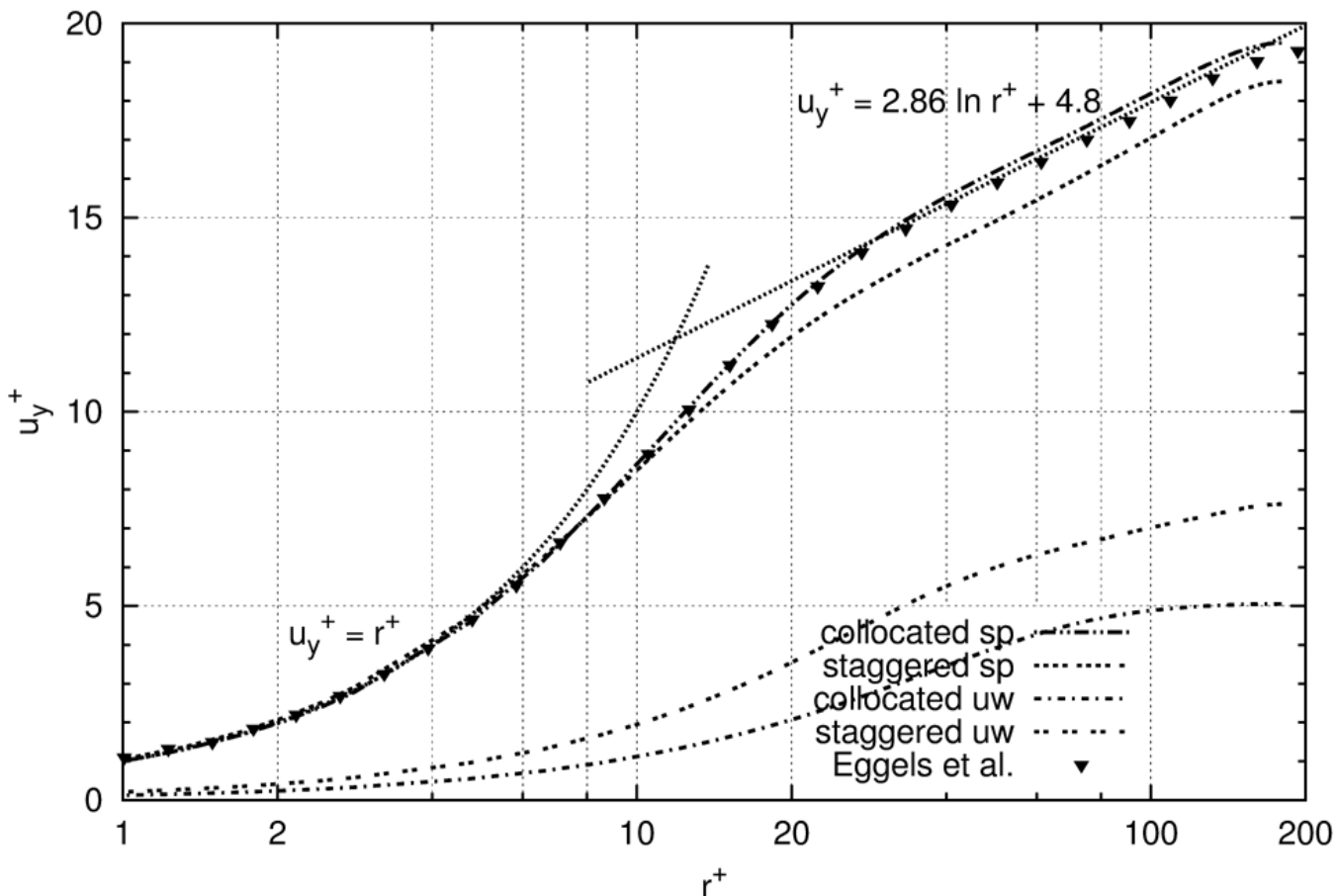
JFF II - CTTC

DNS – Efficient algorithms for HPC needed



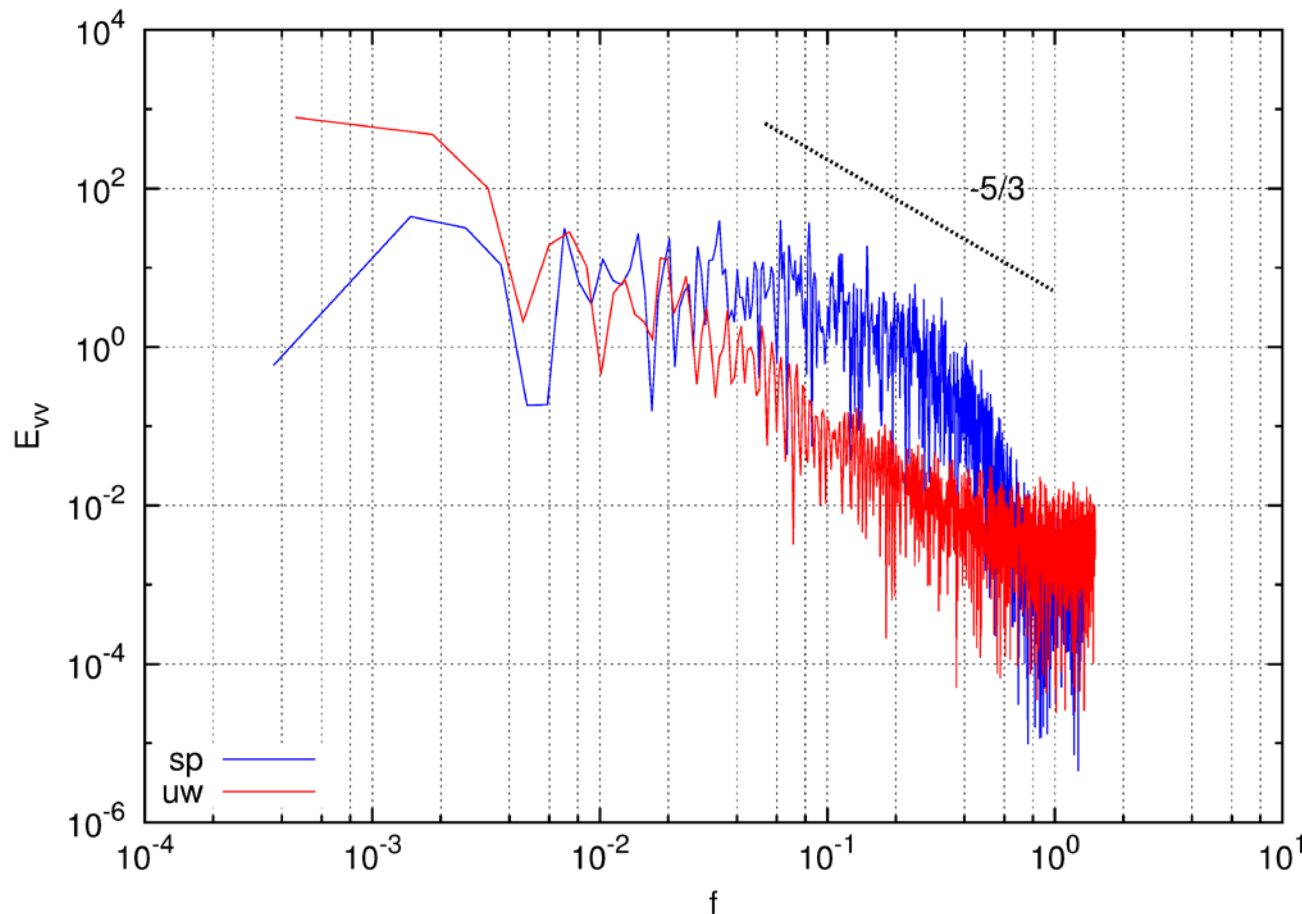
- CPU is increased 4 times ($2048 \rightarrow 8192$)
- Solver time is decreased 3 times (from 0.69s to **0.24s**)
- A **500 M** cv Poisson problem.

DNS – Your numerics are relevant!



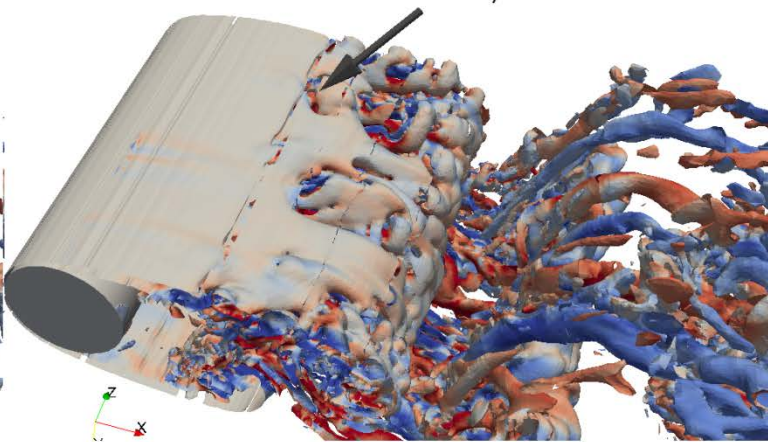
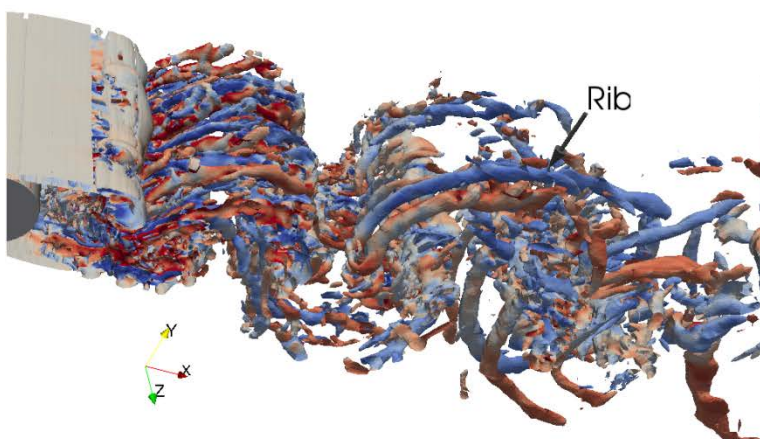
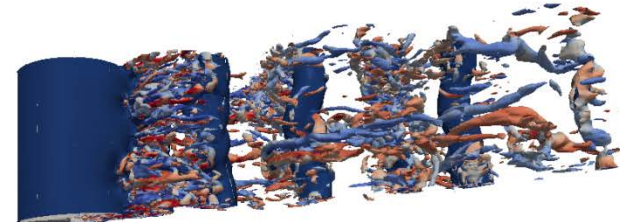
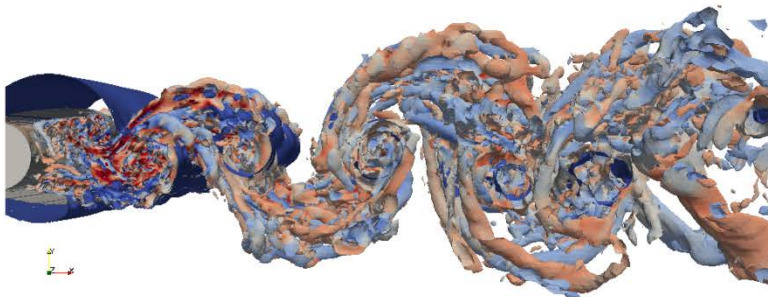
- Pipe flow at Re = 5300
- Mesh size 3 M cv
- Unstructured momentum schemes:
 - Collocated 2 Order
 - Staggered 1 Order
- Convective scheme:
 - Energy conserving (sp)
 - Upwind based (uw)
- **Your NS discretization is going to change the “turbulent behaviour” of your model !!**

DNS – Your numerics can alter the energy behaviour



Spectral distribution of the vertical velocity fluctuation at the centerline of a pipe.

DNS examples – Subcritical circular cylinder (Re 3900)



A large scattering between SoA experiments and DNS

TABLE Statistical flow features. DNS results compared with experimental measurements and numerical results from literature.

	L_z/D	Shedding cycles	f_{vs}	φ_s (°)	L_r/D	$\overline{C_d}$	$-\overline{C}_{pb}$
Present work	π	858	0.215	88	1.36	1.015	0.935
Present work, Mode L	π	250	0.218	87.8	1.55	0.979	0.877
Present work, Mode H	π	250	0.214	88.25	1.26	1.043	0.98
Parnaudeau <i>et al.</i> ¹²	23	250	0.208	88	1.51
Norberg ³⁰ ($Re = 3000$)	67	...	0.22	...	1.66	0.98 ^a	0.88 ^a
Loureco and Shih ^b	21?		...	85	...	0.98	0.9
Dong <i>et al.</i> ³¹ ($Re = 4000$)	11.7	50	1.47
Ma <i>et al.</i> ¹¹ (Case I) (DNS)	2π	100	0.203	...	1.12	0.96	0.96
Ma <i>et al.</i> ¹¹ (Case II) (DNS)	π	100	0.219	...	1.59	0.84	0.88
Tremblay ³² (DNS)	π	50	0.22	85.7	1.3	1.03	0.93
Breuer ¹³ (LES)	π	~22	0.215	87.4	1.372	1.016	0.941
Kravchenko and Moin ¹⁴ (LES)	π	7	0.21	88	1.35	1.04	0.94
Franke and Frank ¹⁵ (LES)	π	40	0.209	88.2	1.64	0.978	0.85
Mahesh <i>et al.</i> ³³ (LES)	π	33	0.218	87.6	1.35	1.0	...
Mani <i>et al.</i> ³⁴ (LES)	π	60	0.206	86.3	...	0.99	0.86

^aTaken from Kravchenko and Moin¹⁴ at $Re = 4020$.

^bData summarised in Mittal.³⁵

Our DNS approach

Single-point measurements have been carried out by positioning probes at different locations. Measurements at those ports have been taken over the whole simulation time. The location of these stations is as follows: $P1 \equiv [x/D = 0.71, y/D = 0.66]$ and $P2 \equiv [x/D = 1.3, y/D = 0.69]$ are located in one of the shear-layers, $P3 \equiv [x/D = 2.0, y/D = 0.0]$ and $P4 \equiv [x/D = 3.0, y/D = 0.0]$ are located in the wake centreline, $P5 \equiv [x/D = 2.0, y/D = 0.59]$ in the wake, $P6 \equiv [x/D = 0.5, y/D = 0.0]$ at the cylinder base, and $P7 \equiv [x/D = -0.171, y/D = 0.465]$ quite close to the laminar boundary layer at about 70° from the stagnation point (see Figure 1).

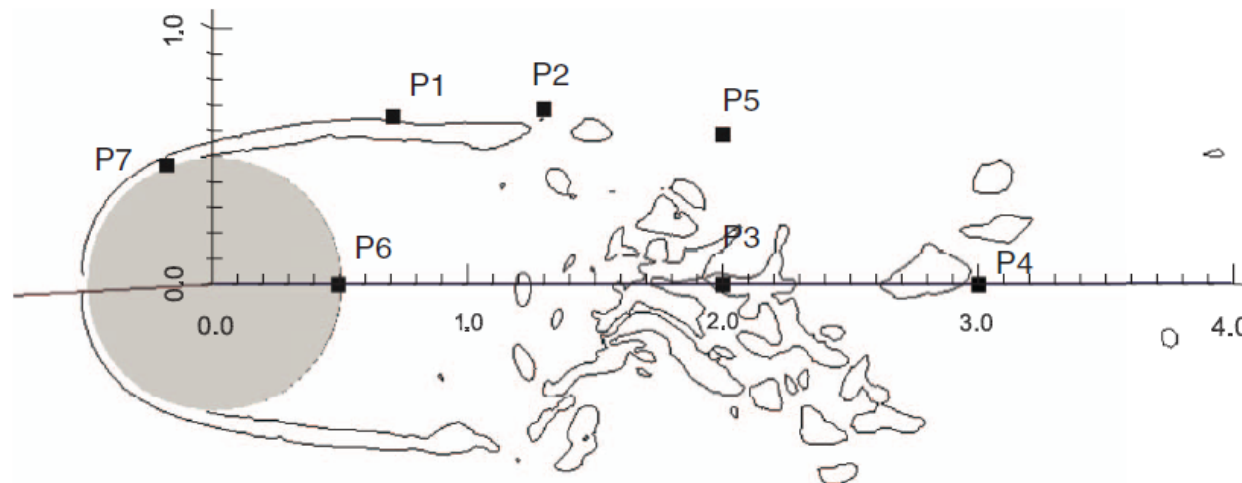


FIG. 1. Location of the computational probes.

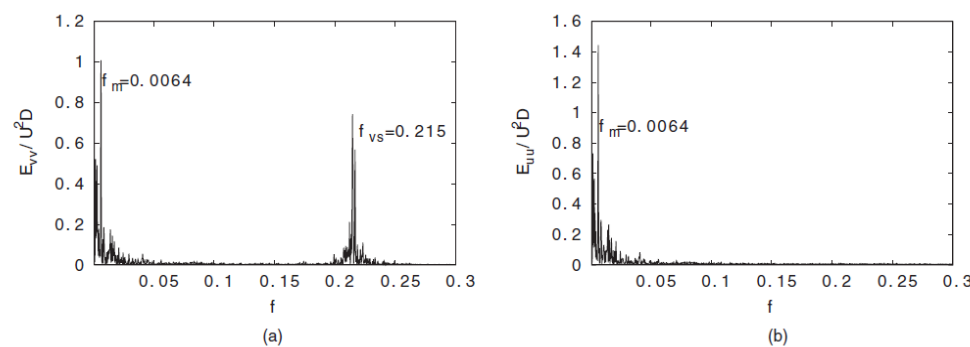
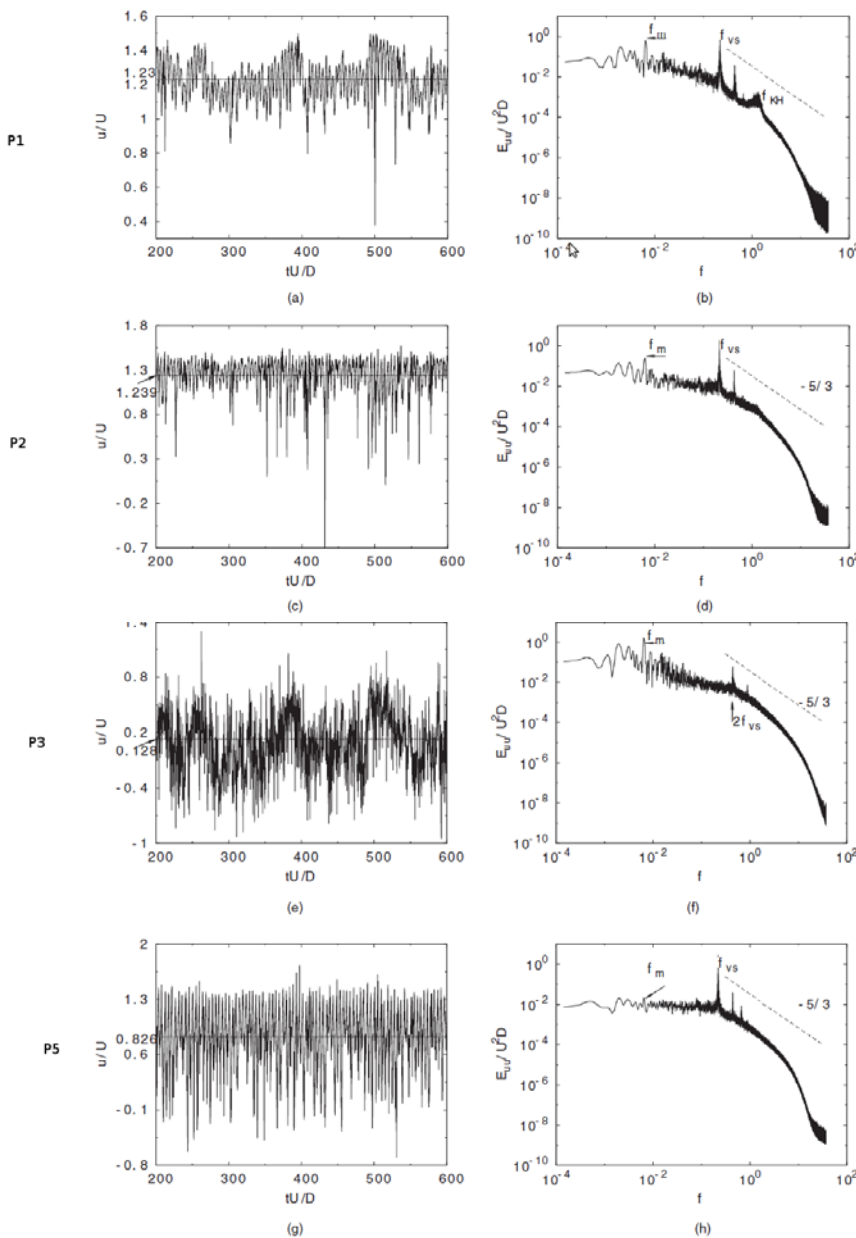
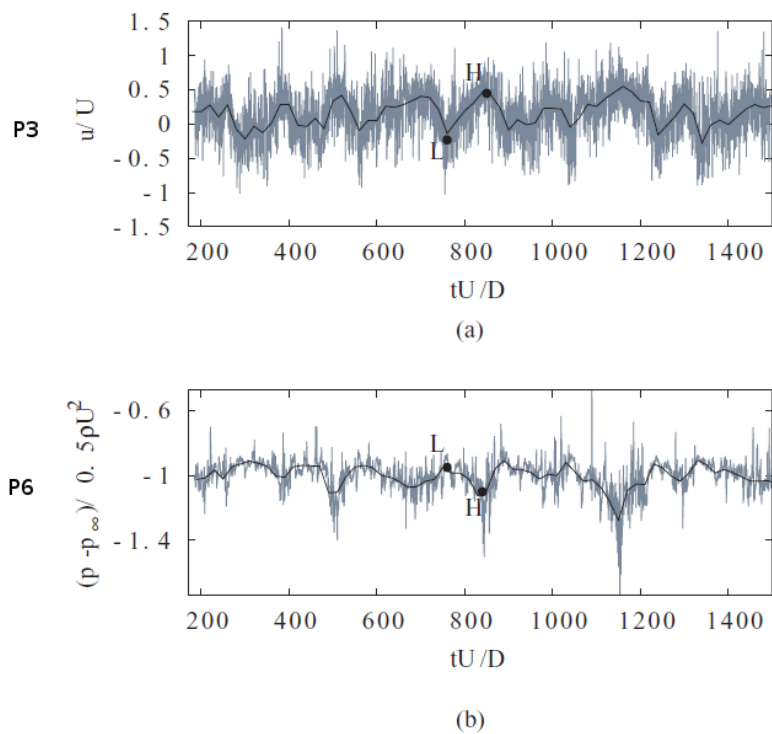
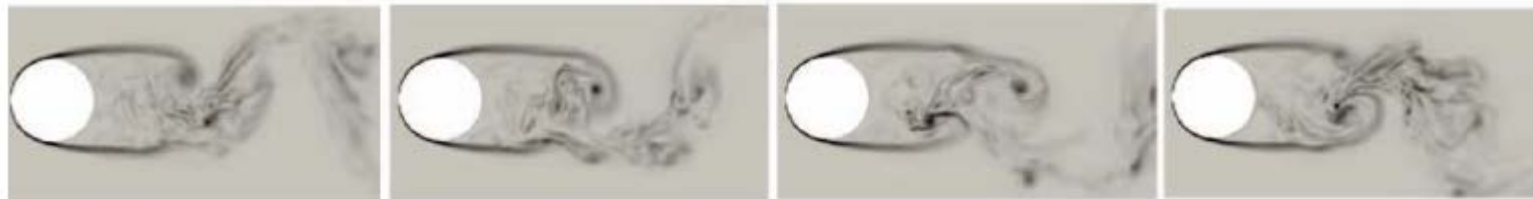


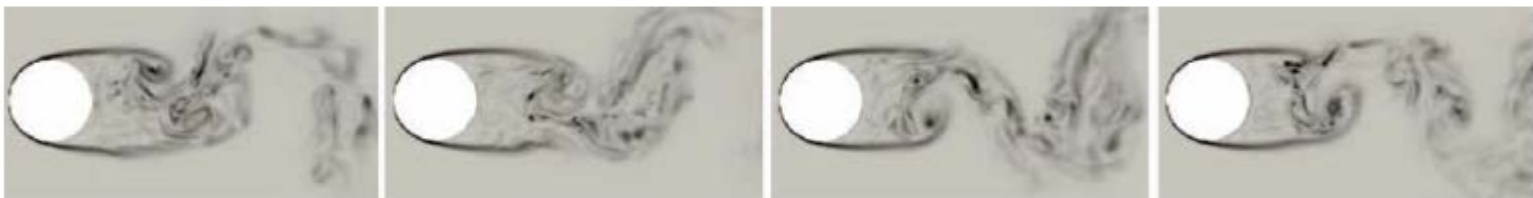
FIG. Energy spectra of the (a) cross-stream velocity at [0.71,0.66] and (b) stream-wise velocity at [2.0,0.0].



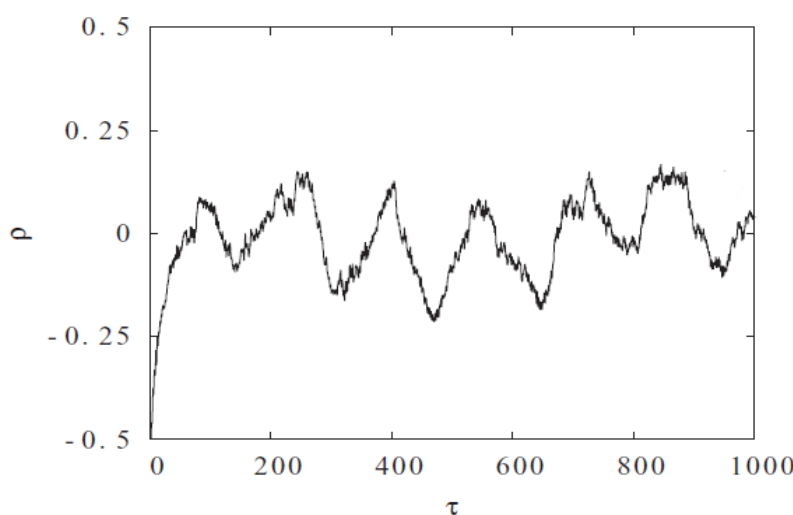
There is a well defined periodic oscillation!



L



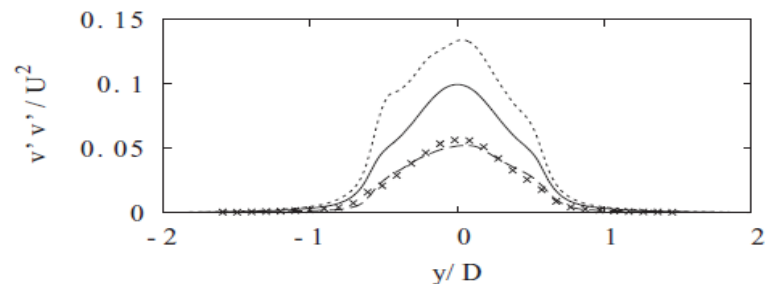
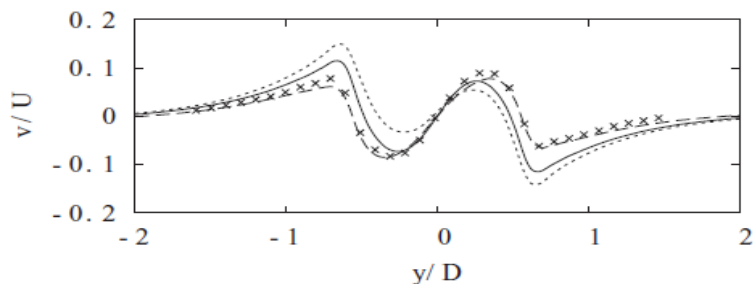
M



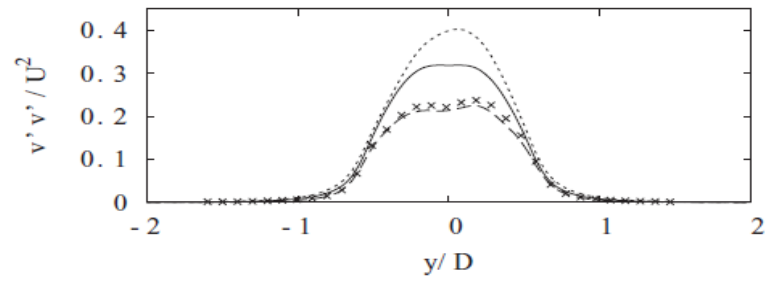
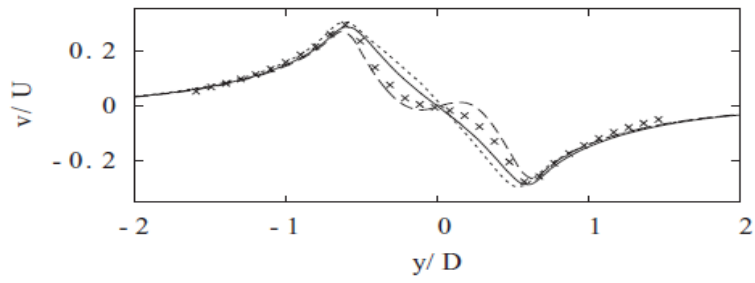
A well-defined periodic oscillation with a period (on average) of $T = 156$ TU can be observed



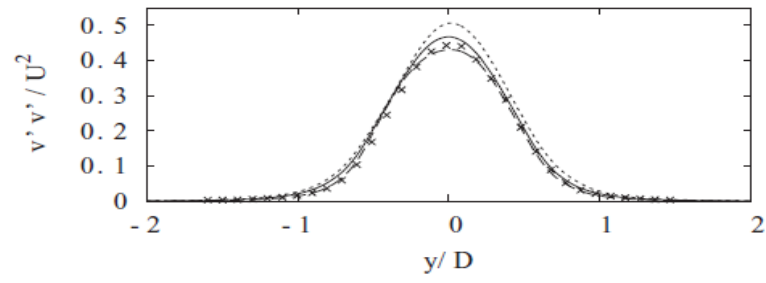
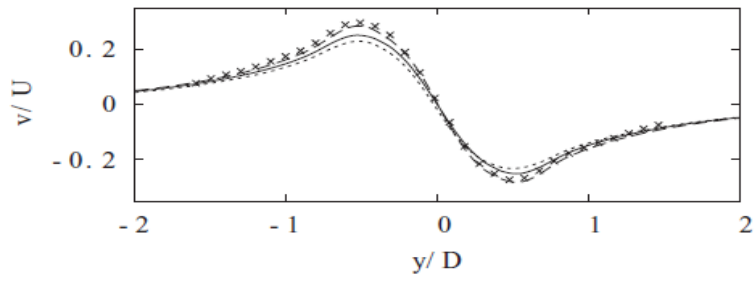
In previous works usually the total averaged time is smaller!!!!



(a)



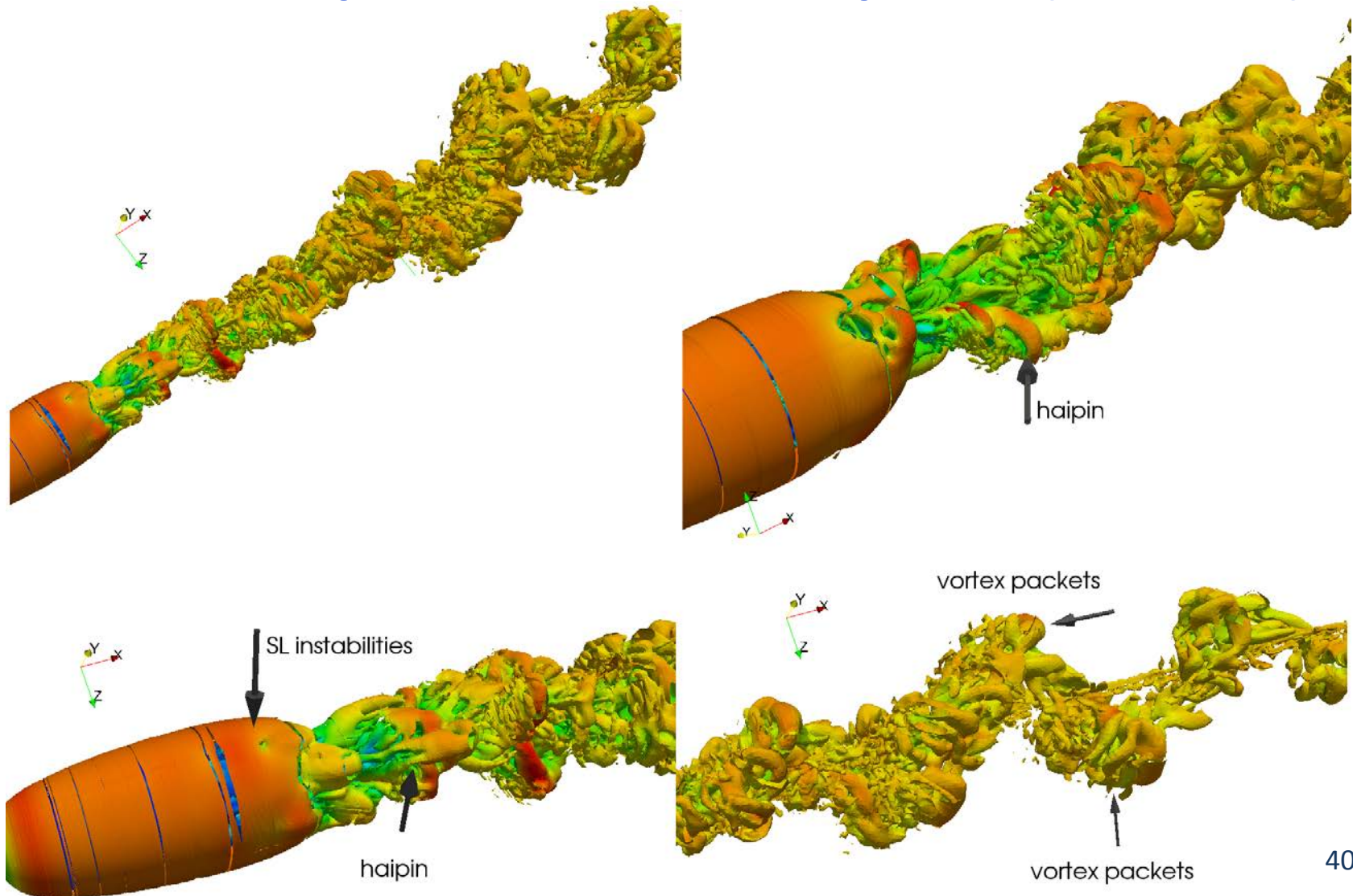
(b)



(c)

FIG. 11. Effects of the recirculation in the wake configuration and comparison with literature results when possible. (Left) Averaged cross-flow velocity profile and (right) its fluctuation at different stream-wise locations: (a) $x/D = 1.06$; (b) $x/D = 1.54$; and (c) $x/D = 2.02$. (Solid line) Long-term averaged solution, (dotted line) Mode H; (dashed line) Mode L; and (\times) experimental results from Parnaudeau *et al.*¹²

DNS examples – Subcritical sphere (Re 3700)



Experimental data is well reproduced by DNS

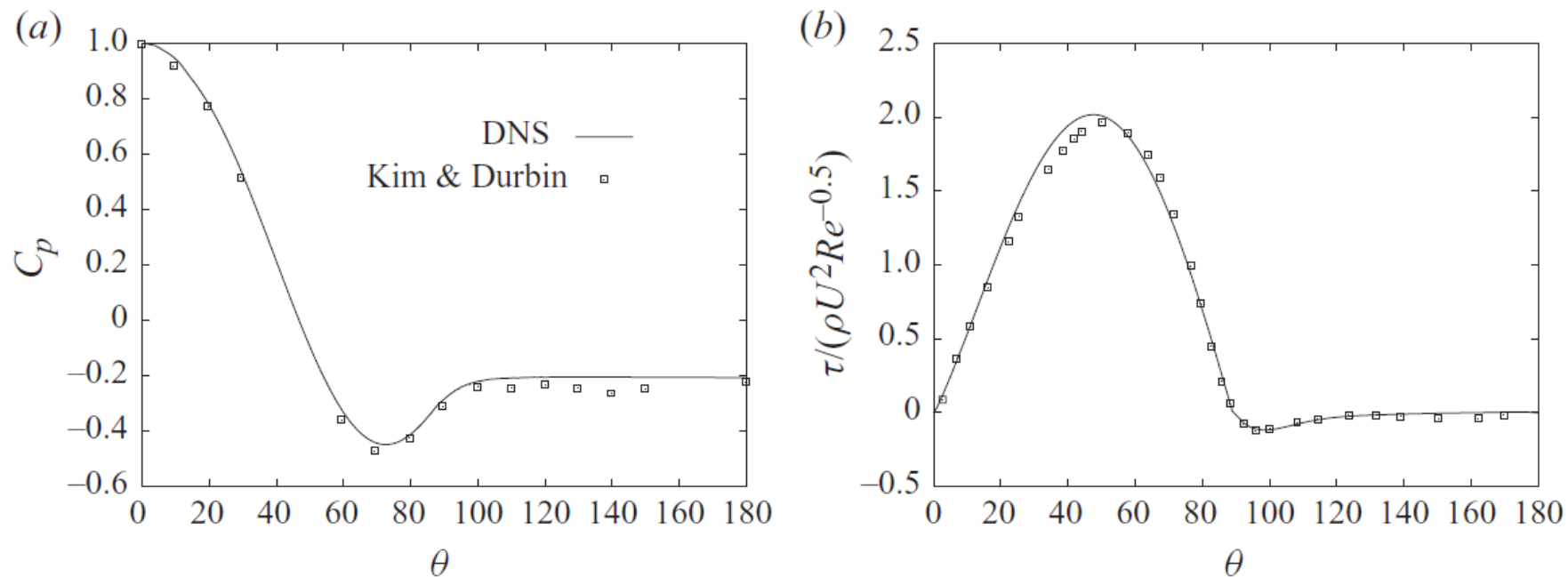


FIGURE Mean profiles around the sphere. (a) Mean pressure distribution compared with experimental results of Kim & Durbin (1988) at $Re = 4200$. (b) Mean skin-friction coefficient compared with numerical results of Seidl *et al.* (1998) at $Re = 5000$.

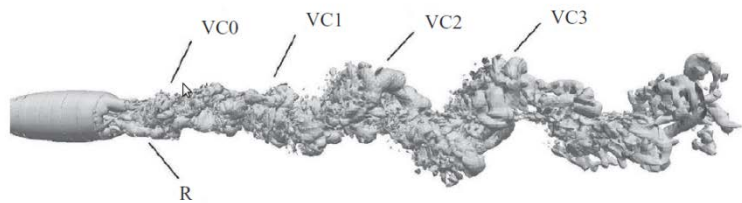
Then, why we need DNS?

The wake exhibits a pronounced helical-like configuration but
how the vortex shedding occur?

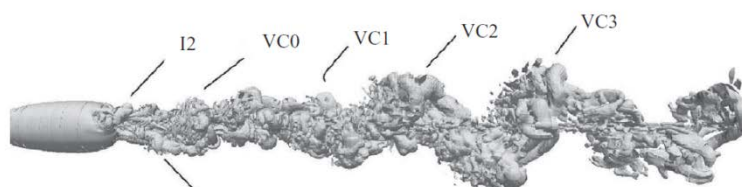
- In his experimental observations, Achenbach (1974) suggested that the vortex shedding occurs at a position around the sphere that rotates with the vortex-shedding frequency.
- Taneda (1978) observed an irregular rotation about the axis of the separation point and the wake.
- LES results from Yun et al. (2006) showed that vortical structures travel downstream nearly straight, and they proposed that the helical-like structure might be related to the wall-pressure changes in the sphere along the azimuthal direction.

Plane X-Y

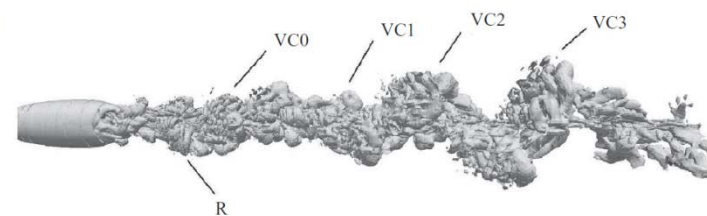
(a)



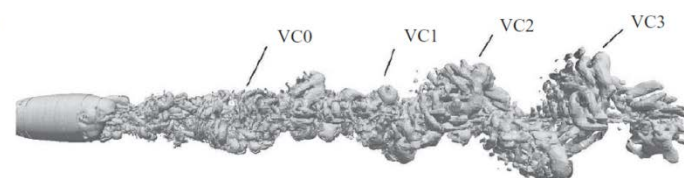
(b)



(c)

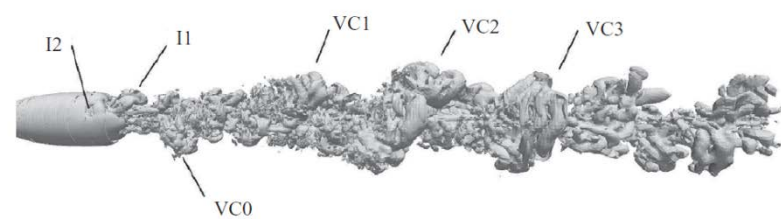


(d)

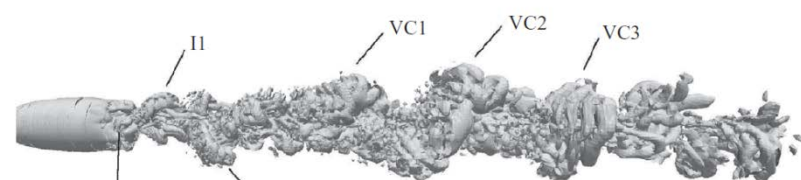


Plane perpendicular X-Y

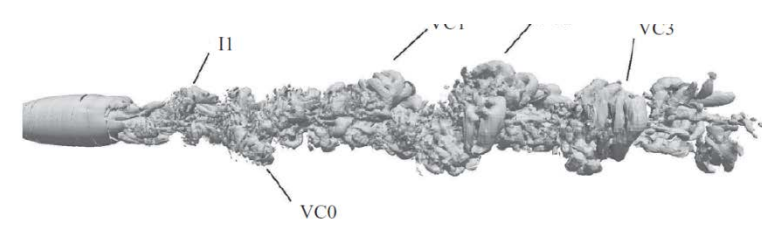
(a)



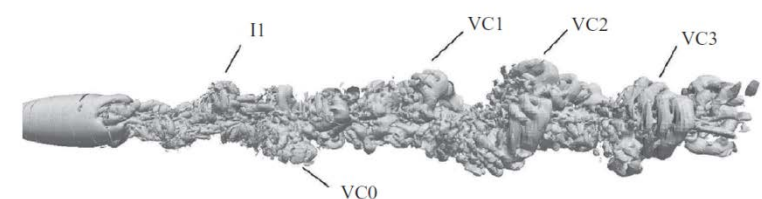
(b)



(c)



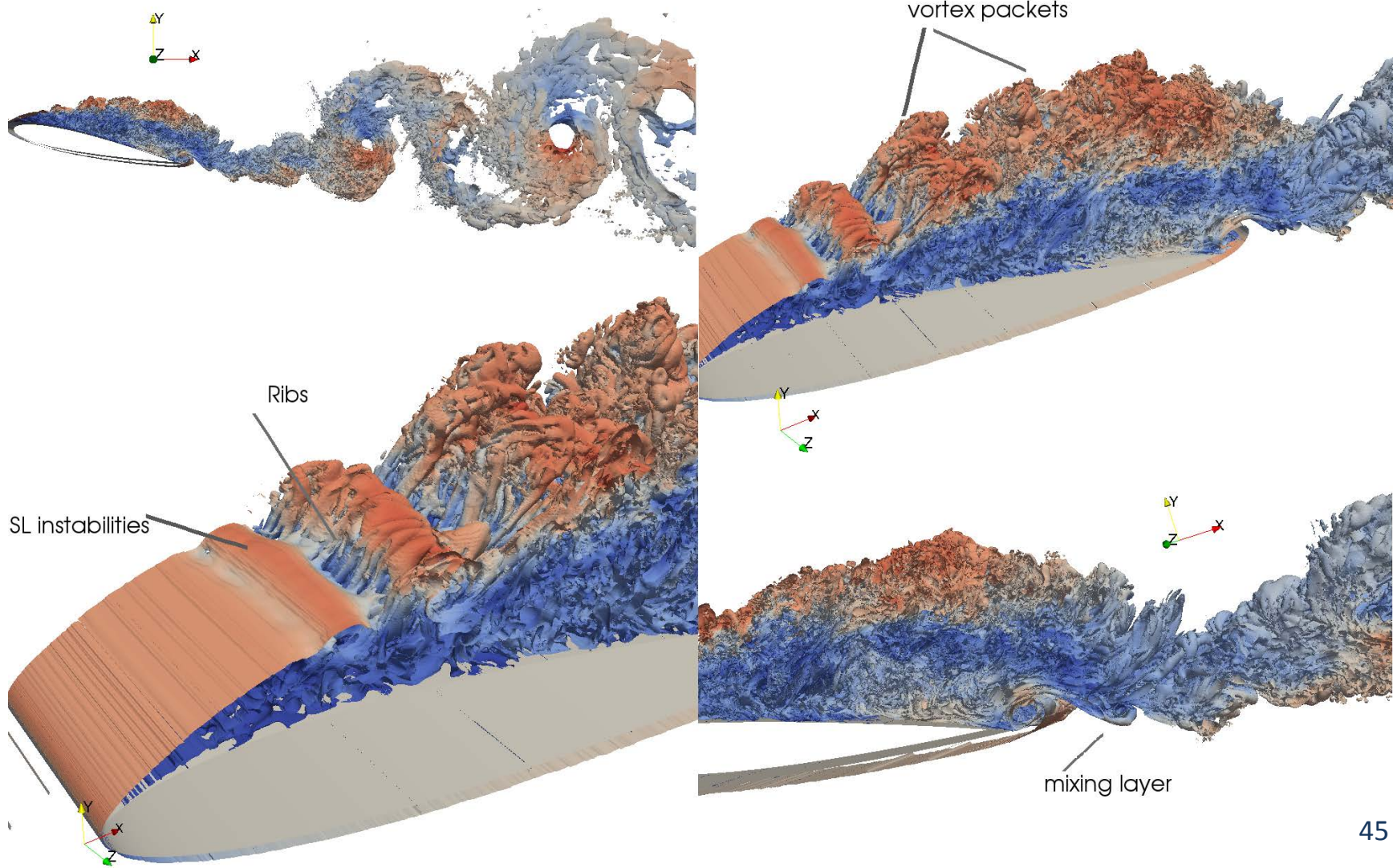
(d)



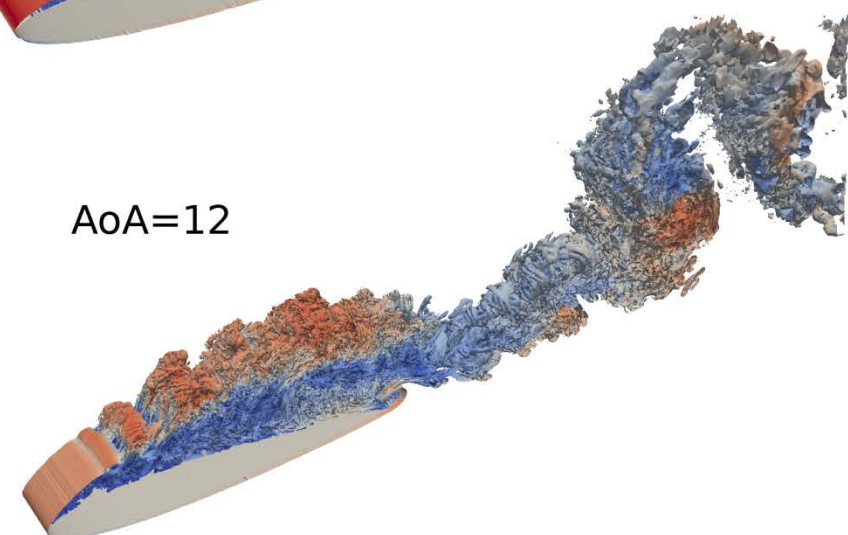
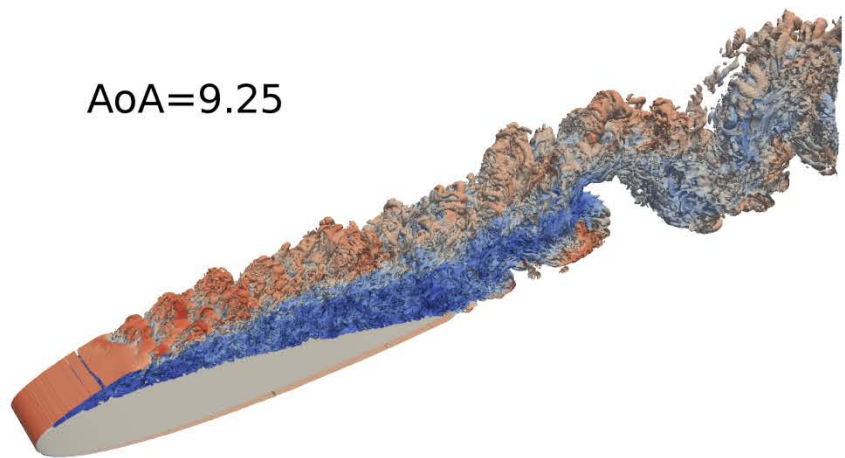
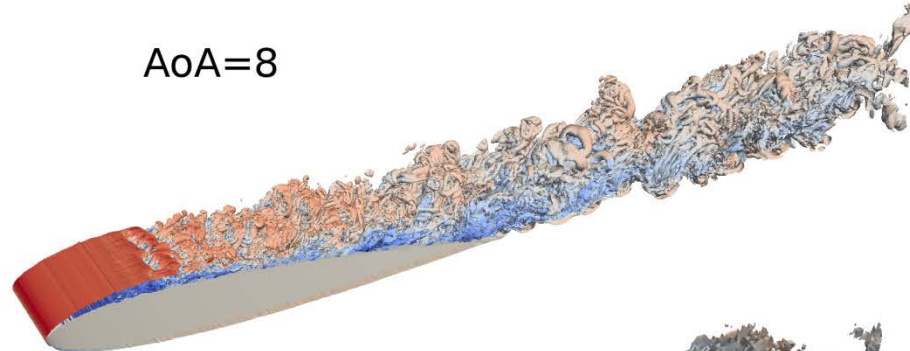
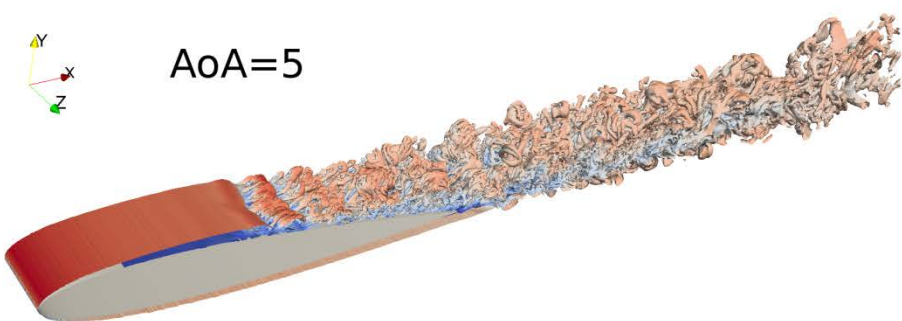
Our DNS findings

- The visualization of the vortex structures over a long period of time shows that the wake has a marked helical-like configuration due to the shedding of vortices at random azimuthal positions in the shear layer.
- During a vortex-shedding period coherent structures are antisymmetric, vortex loops are not strictly detached with 180 degrees of separation.
- Every vortex-shedding period does not occur at the same circumferential location and there is a random change in its azimuthal position, vortices are shed either to the left or to the right of the location of the previous one.
- Large-scale structures move uniformly downstream without circulation in the azimuthal direction, but their relative positions give the appearance of a wavy motion and helical configuration.

DNS – NACA0012 at Re 50 000 stall physics



DNS – AoA simulated



DNS – Obtained results

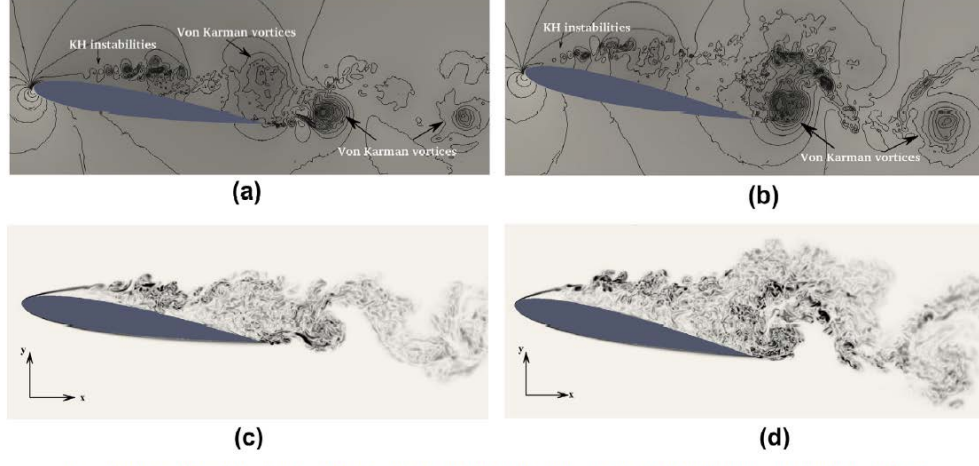


Fig. Instantaneous flow. (a and c) Pressure and vorticity contours for $AOA = 9.25^\circ$. (b and d) Pressure and vorticity contours for $AOA = 12^\circ$.

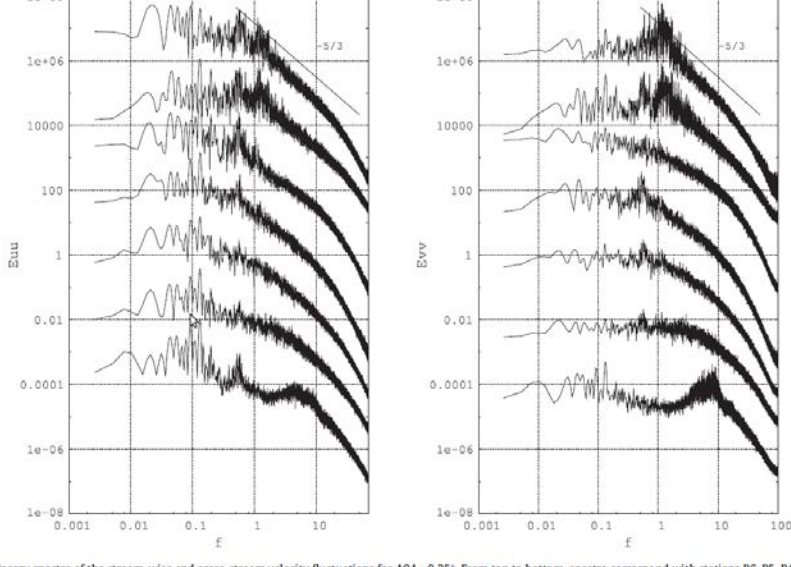


Fig. Energy spectra of the stream-wise and cross-stream velocity fluctuations for $AOA = 9.25^\circ$. From top to bottom, spectra correspond with stations P6, P5, P4, P3, P2, P1, P0 (see Fig. 5 for details).

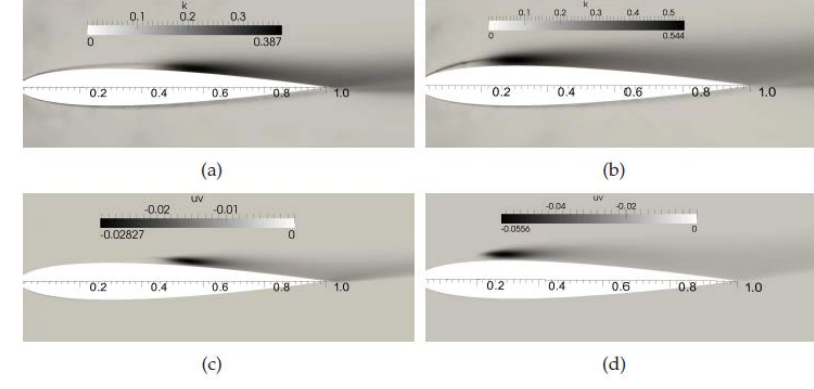


Figure 8.6: Results from DNS simulations: (left) for $AOA = 5^\circ$; (right) for $AOA = 8^\circ$. (a,b) Average turbulent kinetic energy and (c,d) Turbulent shear-stresses in the suction side.

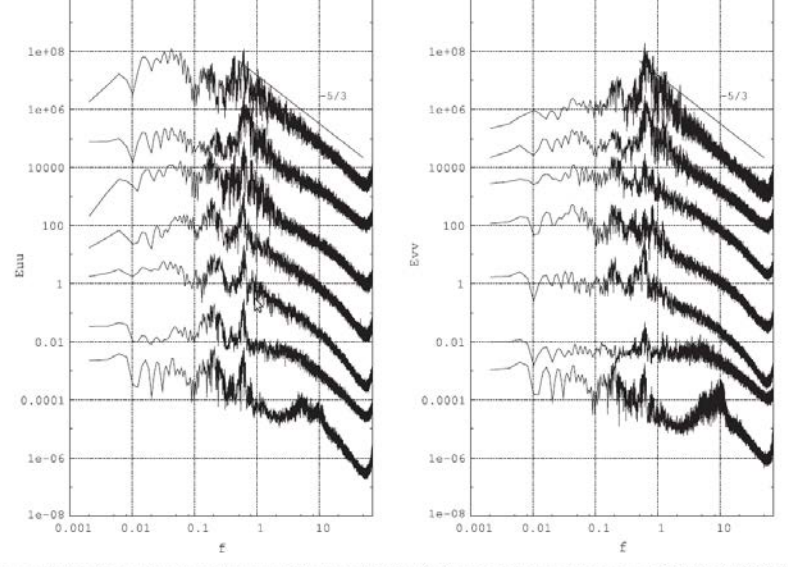


Fig. Energy spectra of the stream-wise and cross-stream velocity fluctuations for $AOA = 12^\circ$. From top to bottom, spectra correspond with stations P6, P5, P4, P3, P2, P1, P0 (see Fig. 5 for details).

LES/RGM – Large Eddy Simulation

- The full energy spectrum can not be computed in most applications. Then, a dynamically less complex mathematical formulation is needed.
- In **LES**, large scales are calculated while the effects of the smallest-scale motions are modelled. Three main steps:
 - **Filtering operation:** $\bar{\phi}(\mathbf{r}, t) = \int_{\Omega} G(\mathbf{r} - \xi, \boldsymbol{\varepsilon}) \phi(\xi, t) d\xi$
 - **Equations for the evolution of the filtered velocity field:**
$$\boldsymbol{\Omega}_c \frac{\partial \bar{\mathbf{u}}_c}{\partial t} + C_c(\bar{\mathbf{u}}_c) \bar{\mathbf{u}}_c - \nu D_c \bar{\mathbf{u}}_c + \rho^{-1} \boldsymbol{\Omega}_c G_c \bar{\mathbf{p}}_c - \boldsymbol{\Omega}_c \bar{\mathbf{f}}_c = C_c(\bar{\mathbf{u}}_c) \bar{\mathbf{u}}_c - \overline{C_c(\mathbf{u}_c) \mathbf{u}_c} = -\mathcal{M}_c \boldsymbol{\mathcal{T}}_c$$
 - **Modelling the SGS stress tensor.** Simplest closure: $\boldsymbol{\mathcal{T}}_c \approx -2\nu_{sgs} \bar{\boldsymbol{\mathcal{S}}}_c + (\boldsymbol{\mathcal{T}}_c : \mathbf{I}) \mathbf{I} / 3$
- LES models considered in this work:
 - Dynamic Smagorinsky LES Model (**Dynamic**)
 - Wall-Adapting Local Eddy-viscosity Model (**WALE**)
 - Verstappen Subgrid-Scale Model (**QR**)
 - Variational Multiscale Method (**VMS**)
- They allow near-wall analysis; wall-distance free; they drive to DNS when the mesh is refined enough.

LES/RGM – Regularization Modelling

- The regularization methods (i.e. smooth approximation of the nonlinearity) basically **alters the convective term to restrain the production of small scales of motion.**
- The first outstanding regularization approach goes back to **Leray [1934]:**

$$\boldsymbol{\Omega}_c \frac{\partial \mathbf{u}_c}{\partial t} + C_c(\bar{\mathbf{u}}_c) \mathbf{u}_c - \nu D_c \mathbf{u}_c + \rho^{-1} \boldsymbol{\Omega}_c G_c \mathbf{p}_c - \boldsymbol{\Omega}_c \mathbf{f}_c = 0$$

- However, in doing so some of the **inviscid invariants** (viz. kinetic energy, enstrophy in 2D and helicity) **are not conserved.**

LES/RGM – Regularization Modelling

- A new approach by R.Verstappen is to approximate the convective nonlinearity in such a manner that the symmetry properties that form the basis for the **conservation of the inviscid invariants are preserved** at the same time as the production of small scales is restrained:

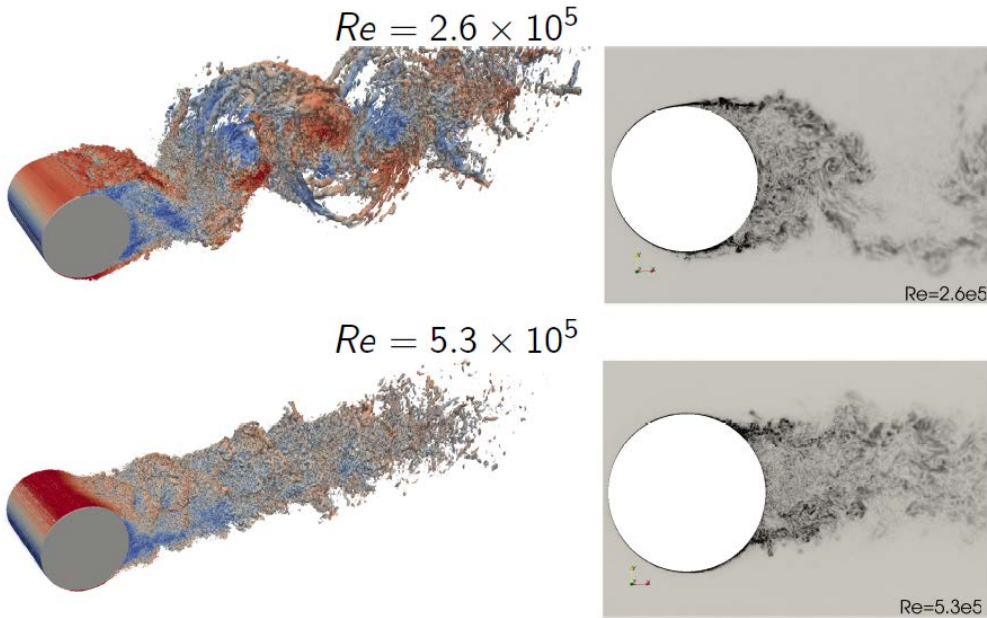
$$C_2(\mathbf{u}, \mathbf{v}) = \overline{C(\bar{\mathbf{u}})\bar{\mathbf{v}}}$$

$$C_4(\mathbf{u}, \mathbf{v}) = C(\bar{\mathbf{u}})\bar{\mathbf{v}} + \overline{C(\bar{\mathbf{u}})\mathbf{v}' + C(\mathbf{u}')\bar{\mathbf{v}}}$$

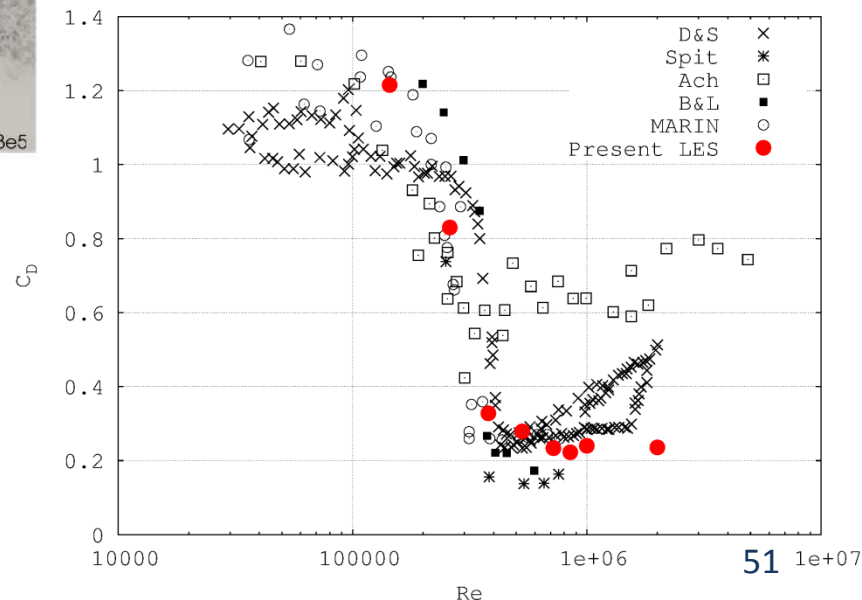
$$C_6(\mathbf{u}, \mathbf{v}) = C(\bar{\mathbf{u}})\bar{\mathbf{v}} + C(\bar{\mathbf{u}})\mathbf{v}' + C(\mathbf{u}')\bar{\mathbf{v}} + \overline{C(\mathbf{u}')\mathbf{v}'}$$

where $\overline{(\cdot)}$ represents a normalised self-adjoint linear filter with filter length ε , and $\mathbf{u}' = \mathbf{u} - \bar{\mathbf{u}}$ are the residual velocities.

LES/RGM – basic research – drag crisis

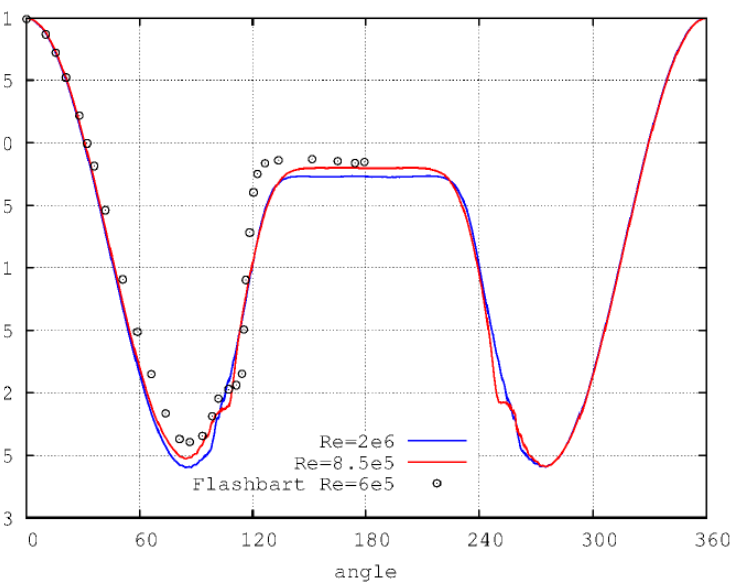
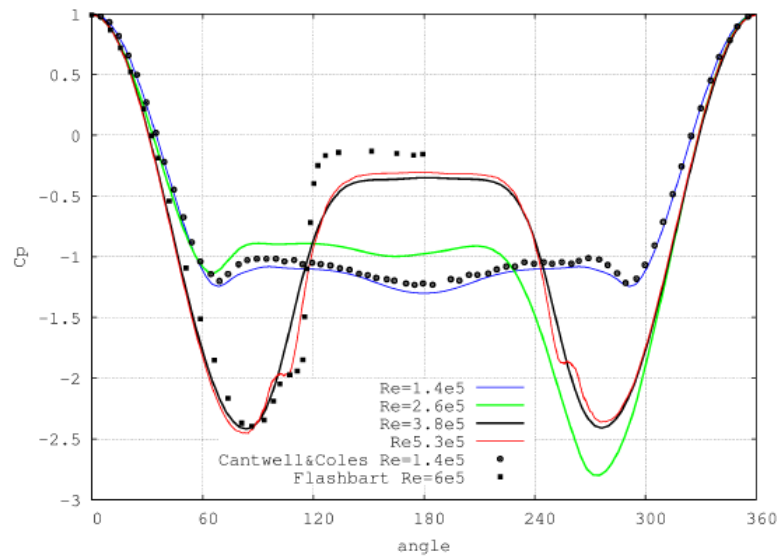


Re	NCV_t [MCVs]	$N_{CV\ plane}$	N_{planes}	L_z
1.4×10^5	38.4	299683	128	1.5D
2.6×10^5	38.4	299683	128	1.5D
3.8×10^5	48.6	379950	128	1.5D
5.3×10^5	64	500516	128	1.5D
7.2×10^5	83.2	650432	128	D
8.5×10^5	89.5	698949	128	D
1×10^6	157.6	820803	192	D
2×10^6	198.3	1032952	192	D
4×10^6	329.7	1288154	256	D



In the **critical** regime, the transition to turbulence in the boundary layer causes the delaying of the separation point and, an important **reduction** of the **drag force** on the cylinder surface known as the **Drag Crisis**

LES/RGM – basic research – drag crisis



Re	C_D	$-C_{p_b}$	$\varphi_{sep} [^\circ]$	$\varphi_{Pmin} [^\circ]$
1.4×10^5	1.215	1.3	95.5	68.5
2.6×10^5	0.83	0.984	95/252	70/280
3.8×10^5	0.328	0.347	102	83.8
5.3×10^5	0.247	0.15	121	86
Cantwell&Coles $Re=1.4e5$	1.237	1.21	-	-
Achenbach $Re=2.6e5$	-	-	94	-

LES/RGM – basic research – DHC at extreme Ra

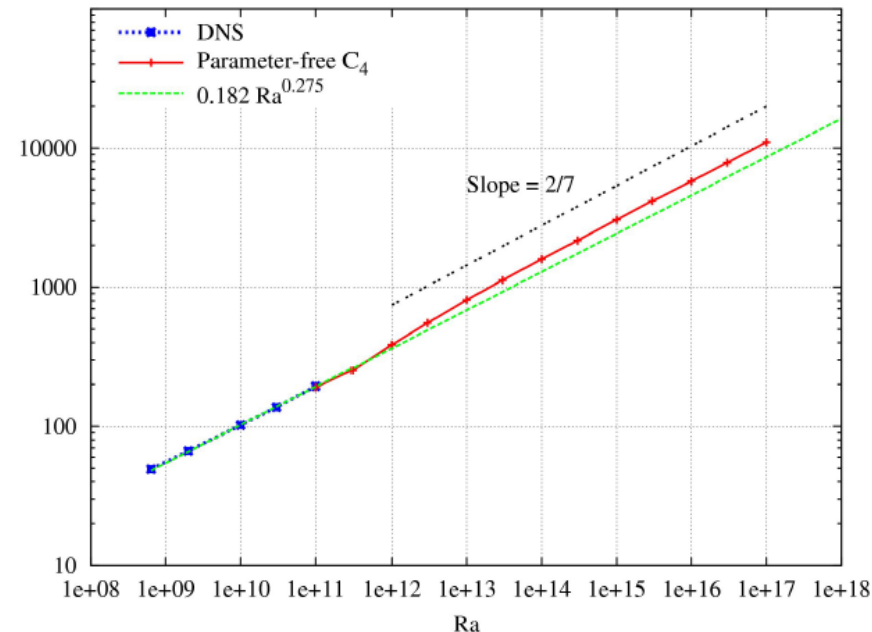
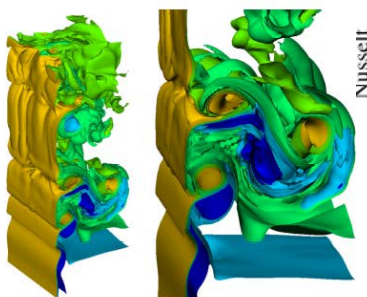


Some details about DNS:

- Mesh size: $128 \times 318 \times 862$
- ≈ 1 months - 128 CPUs
- 4th-order symmetry-preserving scheme
- $A_z = 5$

Complexity of the flow:

- Boundary layers
- Stratified cavity core
- Internal waves
- Recirculation areas
- Regularization model C_4 is tested.
- Two coarse meshes are considered

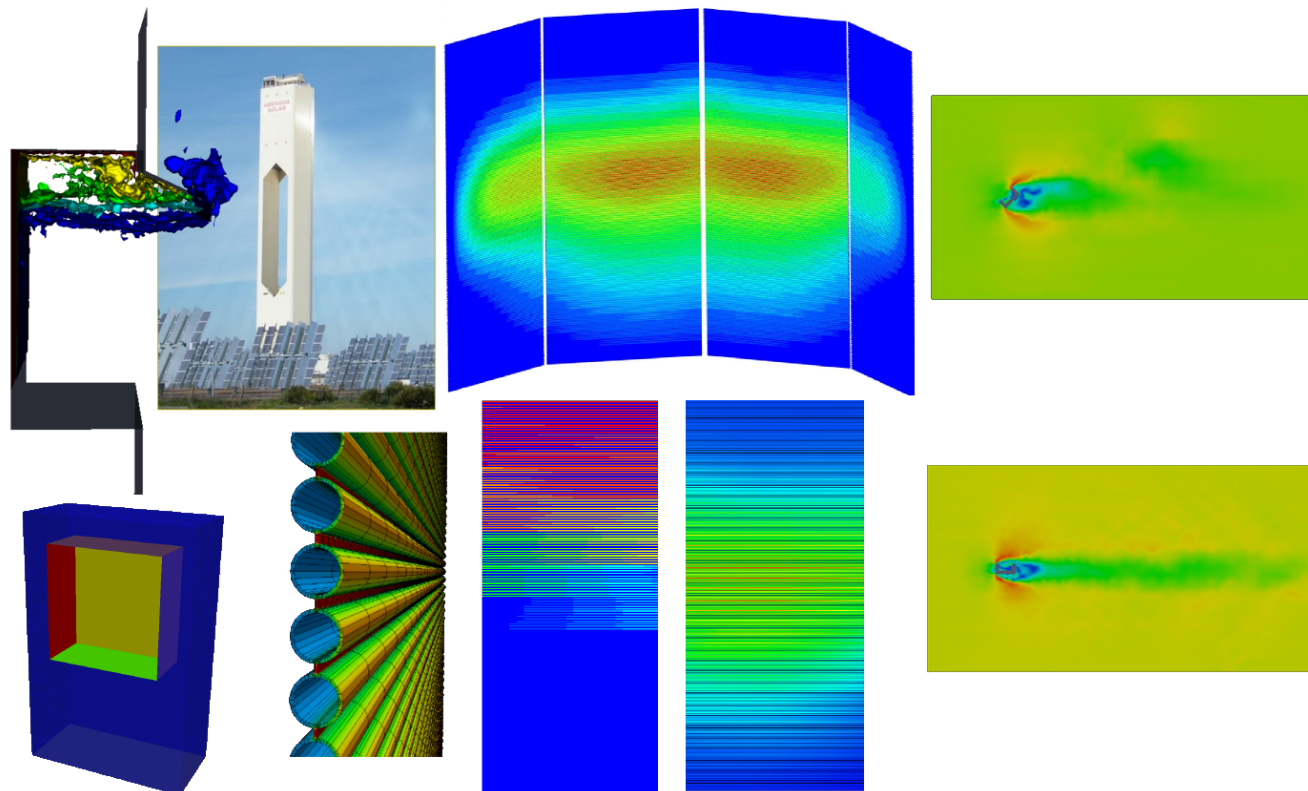


	DNS	RM1		RM2	
	Mesh	$128 \times 318 \times 862$	$8 \times 20 \times 54$	$8 \times 14 \times 38$	No C_4 model
Nu	154.5	194.1	157.5	210.5	159.4
Nu_{max}	781.5	535.2	682.6	558.2	711.8
Nu_{min}	10.5	86.9	18.1	93.7	15.1

LES/RGM – Industrial applications - CSP

LES technology applied for the optimal design of the PS20 solar receivers

- High fidelity CFD simulations of the tower and its interaction with the wind
- Multi-physics simulation of the reviver including the steam generation coupled with the plant dynamics



LES/RGM – Industrial applications - CSP

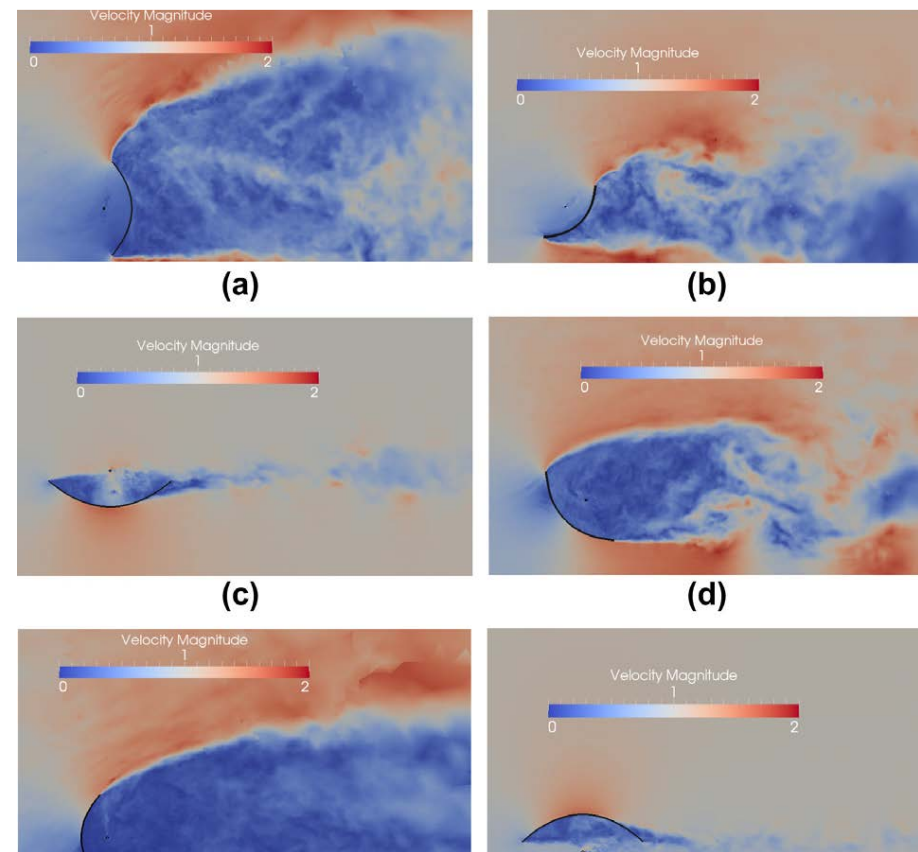
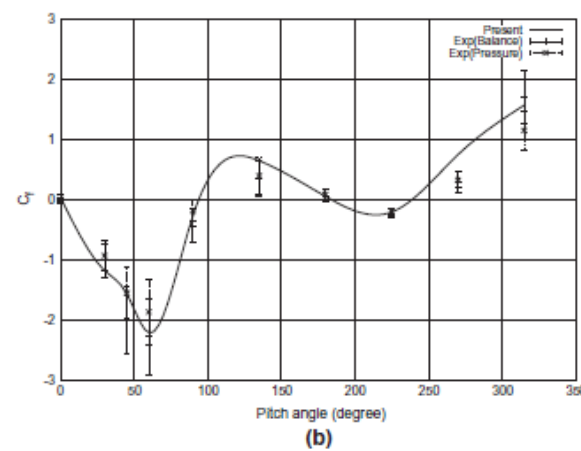
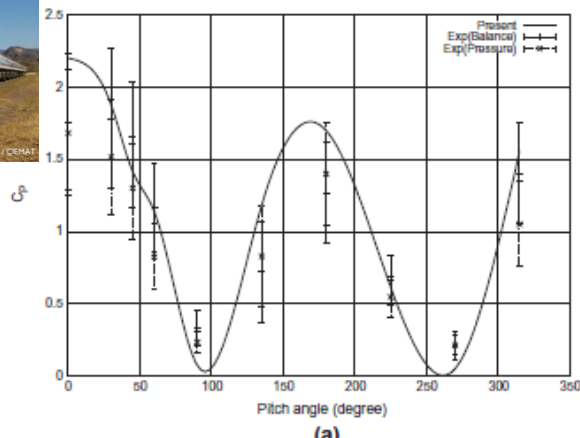
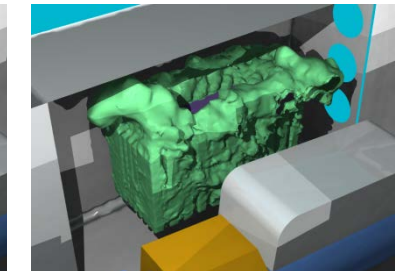
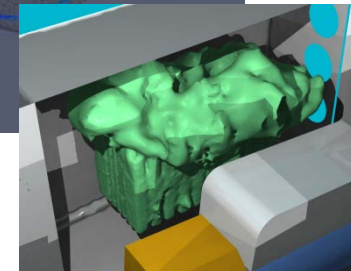
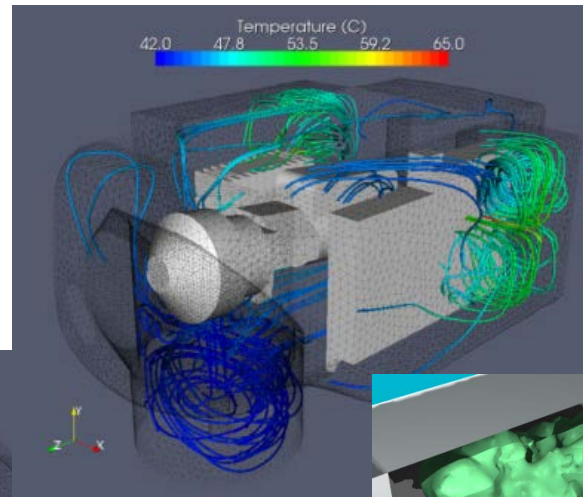
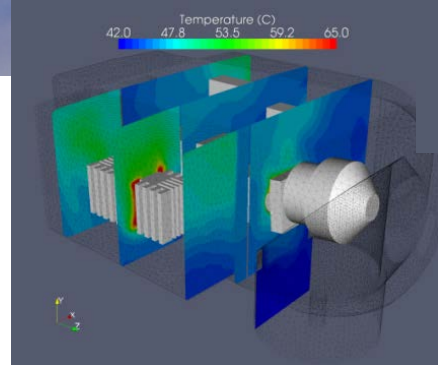


Fig. 5. Predicted and measured aerodynamic parameters for Eurotrough PTC (a) drag and (b) lift coefficients.

LES/RGM – Industrial applications - wind

Numerical simulation of the thermal and fluid dynamic analysis of nacelle and wind turbines

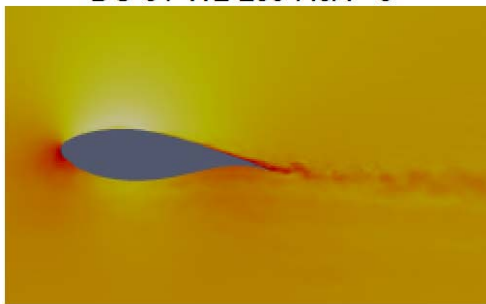
- A finned transformer delivers the electric output of the WTG
- The air is pumped out by a set of fans by the transformer zone
- Complex flow due to concurrent natural and turbulent flow



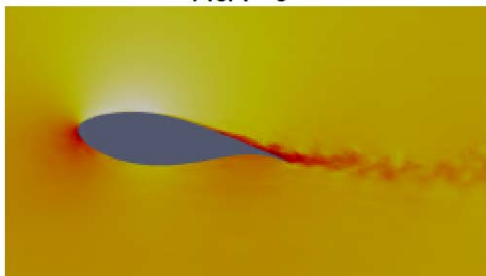
LES of the airflow inside wind generator turbine nacelle for a Re number of 6.10^5 , using only 3 CPUs and 1.1 million control volumes.

LES/RGM – Industrial applications - wind

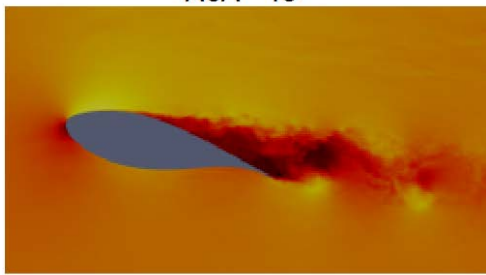
DU-91-W2-250 AoA= 6°



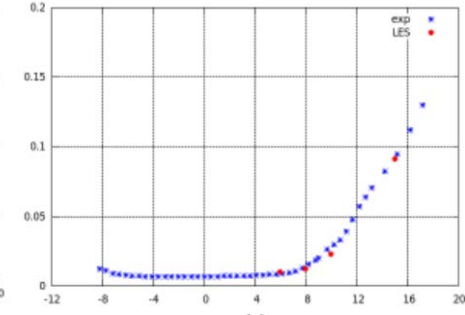
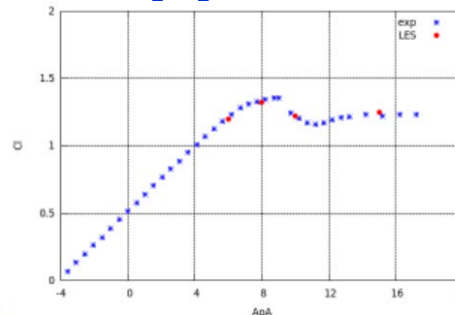
AoA= 9°



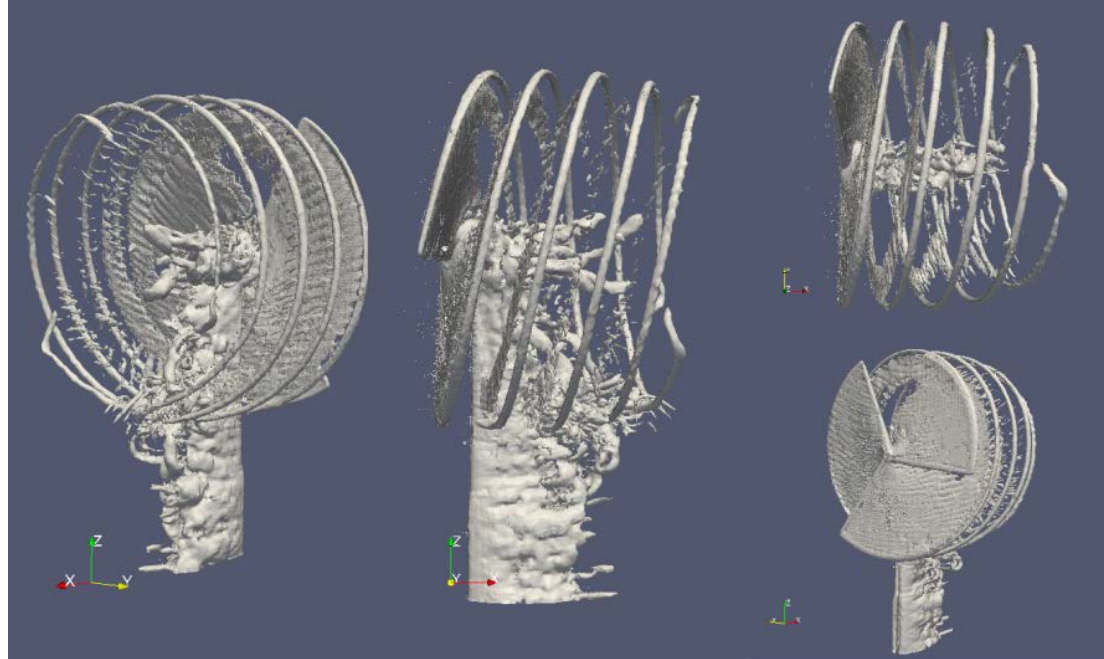
AoA= 15°



Snapshots of the instantaneous flow over the DU-91-W2-250 profile at different AoA and Re number of 1M



Numerical results for the DU-93-W-210 profile and Re number of 3M



Snapshots of the instantaneous flow over the OFFWINDTECH turbine using a 70 M mesh and 512 CPUs

LES/RGM – Industrial applications – heat exchangers

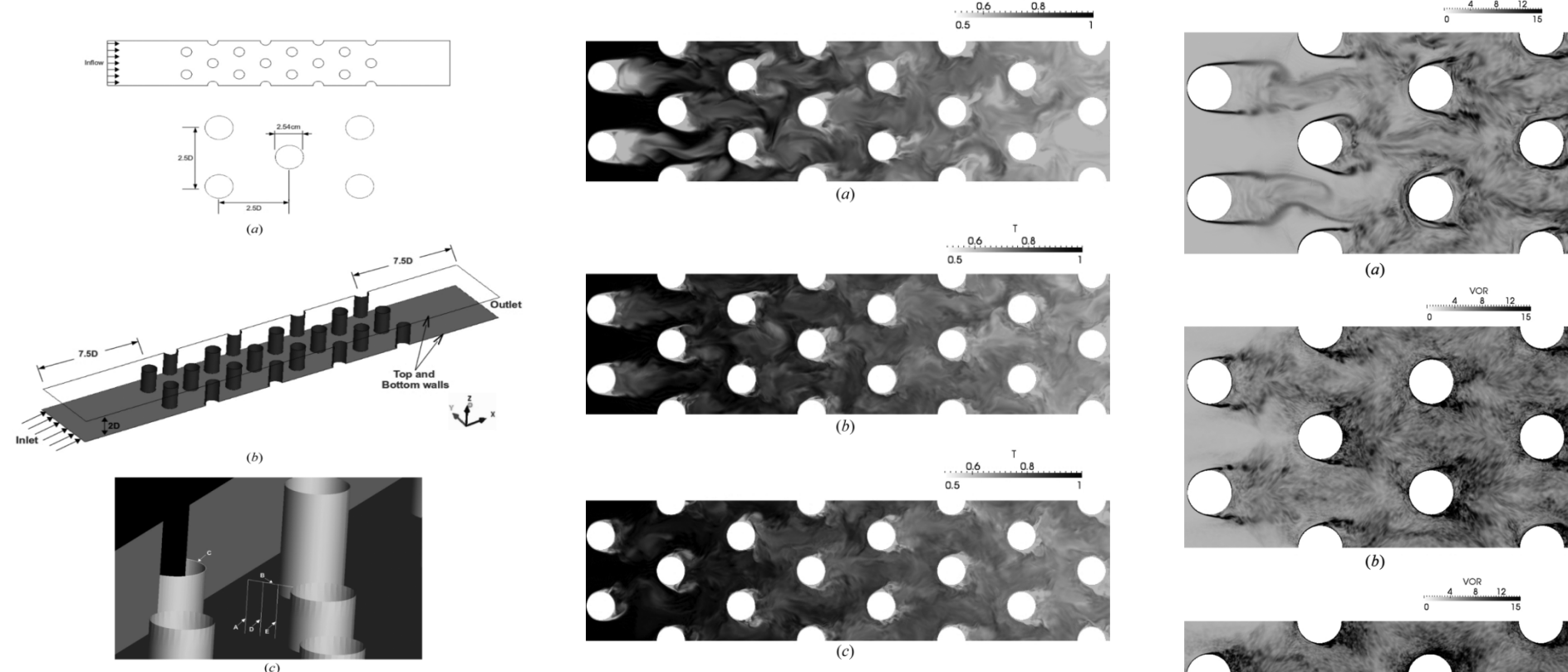
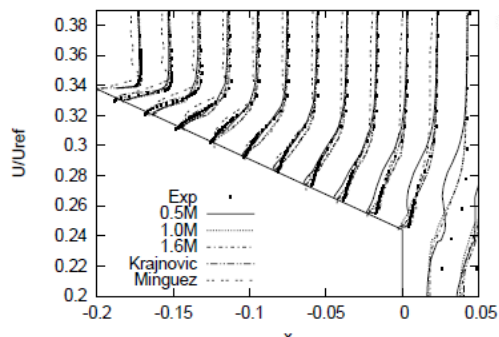


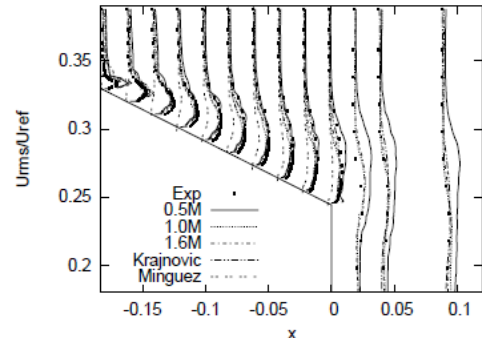
Table 2. Averaged end wall Nusselt number

Re	Correlation Metzger et al. [28]	Experiment Ames et al. [6]	Numerical Delibra et al. [13]	LES QR	LES WALE	LES VMS
3,000	23.82	—	—	21.49	21.91	21.34
10,000	54.33	54.1	44.3 ^{LES}	53.75	51.16	43.45
30,000	115.31	111.5	84.2.3 ^{LES}	110.60	115.45	112.59

LES/RGM – Industrial applications – automotive



(a)



(b)

Figure 4: Mesh study for the Ahmed car. (a) Average stream-wise velocity and (b) its fluctuations, over the slant wall in the mid plane.

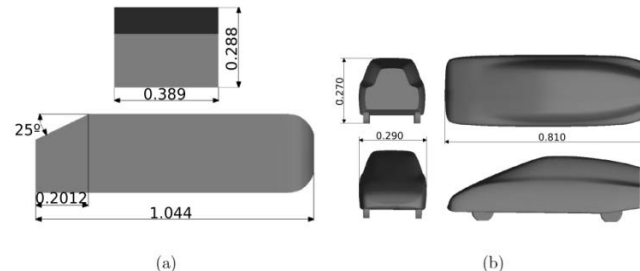


Figure 1: Model dimensions - Units in meters. (a) Ahmed car; (b) Asmo car

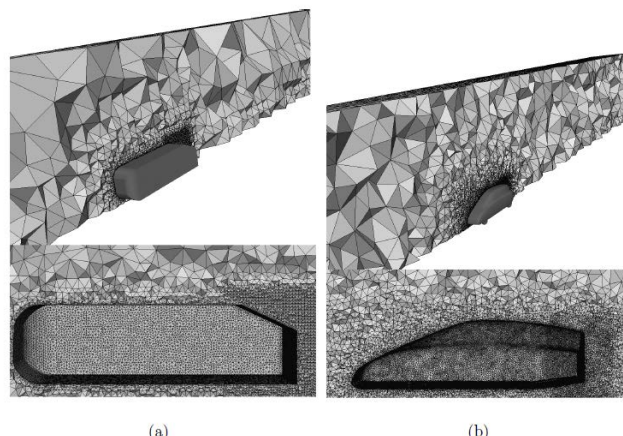
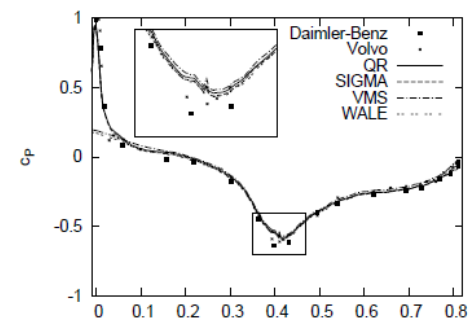
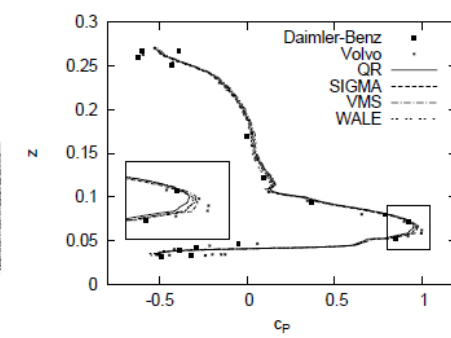


Figure 3: Visualization of the mesh in the channel. (a) Ahmed car; (b) Asmo car.



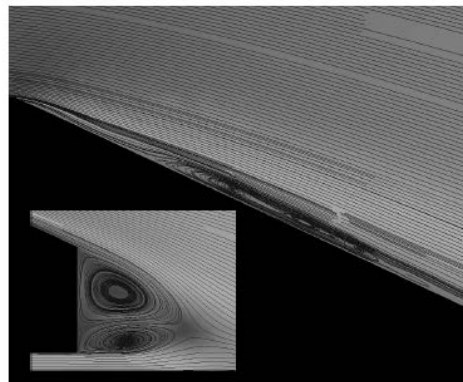
(a)



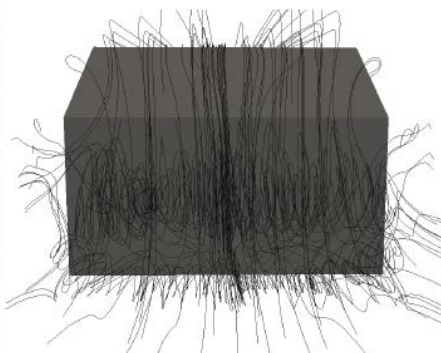
(b)

Figure 9: Pressure coefficients for the Asmo car. (a) In the roof. (b) In the frontal section.

LES/RGM – Industrial applications – automotive



(a)



(b)

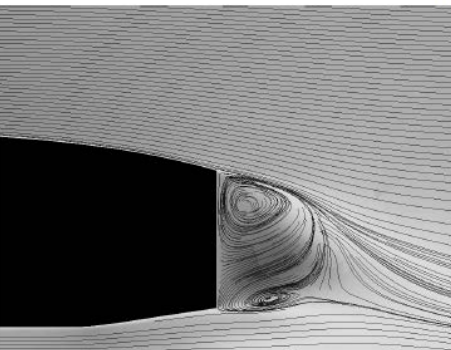
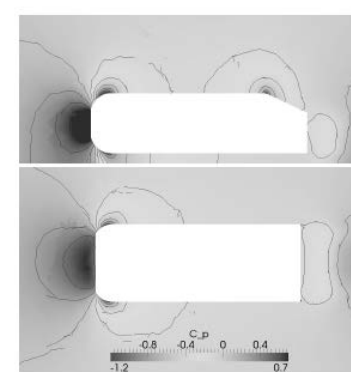
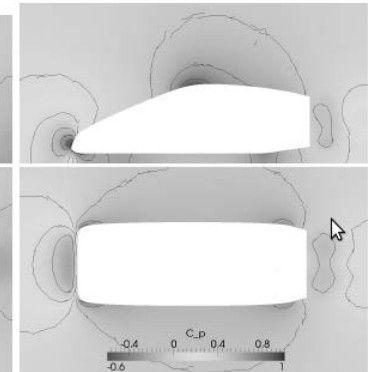


Figure 12: Recirculation bubble behind the geometries.(a) Ahmed car. (b) Asmo car.

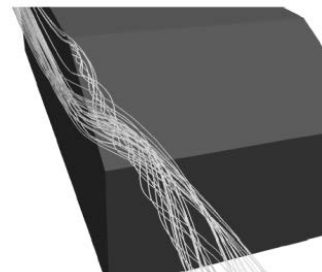


(a)

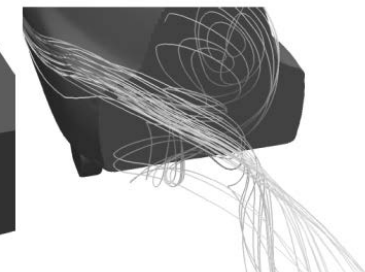


(b)

Figure 13: Time-averaged non-dimensional pressure contours.(a) Ahmed car. (b) Asmo car.



(a)



(b)

Figure 11: Time-averaged streamlines in the back of the car models. (a) Ahmed car. (b) Asmo car.

LES/RGM – Industrial applications – automotive



(a)



(b)

Figure 14: Instantaneous Q-isosurfaces in the front of the Ahmed car, $Q = 20$. (a) 1.5×10^6 CV mesh. (b) 4×10^6 CV mesh



(a)

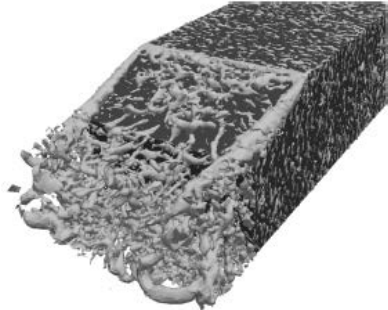


(b)

Figure 16: Instantaneous Q-isosurfaces in the front of the Asmo car, $Q = 20$. (a) 2.8×10^6 CV mesh. (b) 5.3×10^6 CV mesh.

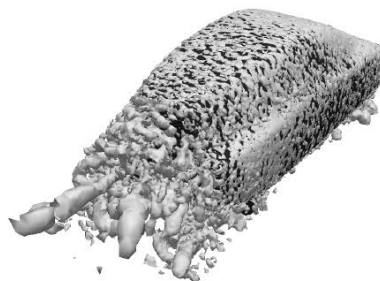


(a)

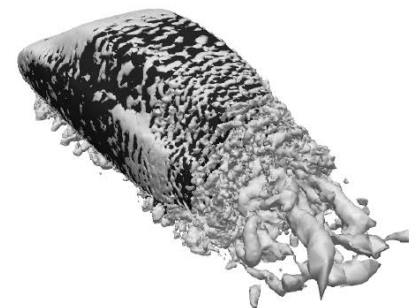


(b)

Figure 15: Instantaneous Q-isosurfaces in the rear of the Ahmed car, $Q = 200$. (a) 1.5×10^6 CV mesh. (b) 4×10^6 CV mesh



(a)



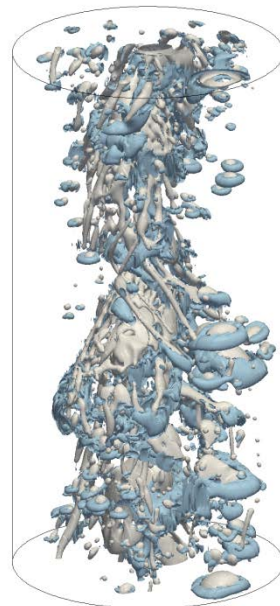
(b)

Figure 17: Instantaneous isosurfaces in the back of the Asmo car. $Q = 200$. (a) 2.8×10^6 CV mesh. (b) 5.3×10^6 CV mesh.

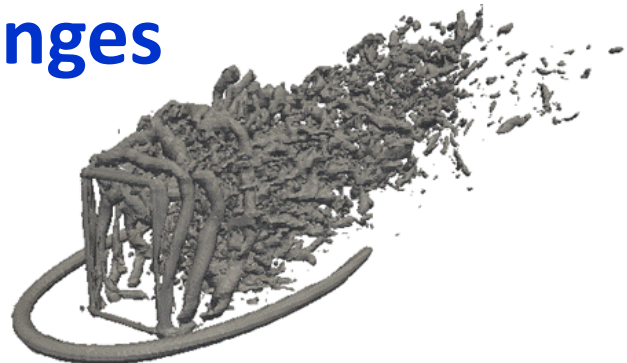
LES/RGM – Challenges



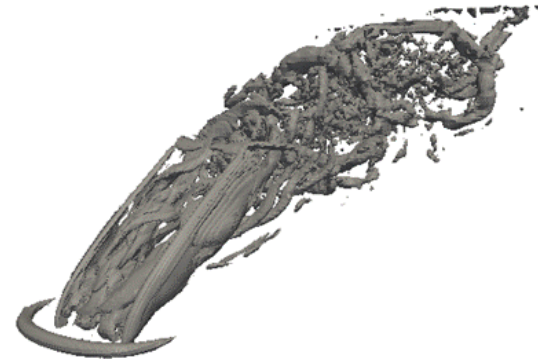
LES simulation of a DLR diffusion flame using FPV approaches with a 2M cv mesh and 96 CPUs



DNS of gravity-driven bubbly flow using 13 million cv and 386 cpu



(a) Early stage.



(b) Developed stage.

Fig. 1: LES of a shell subjected to a turbulent cross-flow.